JOURNAL OF GEOPHYSICAL RESEARCH, VOL. 106, NO. C7, PAGES 14,143–14,163, JULY 15, 2001

Hydrophysical experiment "Megapolygon-87" in the northwestern Pacific subarctic frontal zone

Nikolai A. Maximenko,[1,2] Mikhail N. Koshlyakov,[2] Yury A. Ivanov,[2] Maxim I. Yaremchuk,[1,2] and Gleb G. Panteleev[2,3]

Abstract. The purpose of this paper is to familiarize readers with major results and findings of the biggest multi-institutional Soviet hydrophysical experiment, "Megapolygon-87," conducted in the northwestern Pacific Subarctic Frontal Zone in June–October 1987. Six large-scale, high-spatial-resolution conductivity-temperature-depth (CTD) surveys (1653 profiles) and numerous moorings (an array of 177 buoys deployed within a 500 km × 500 km area) with current meters at four depths provided unique observations of frontal structure, mesoscale and submesoscale eddies, and their evolution and interaction with each other. We discuss errors induced in the velocity records by surface waves and show how they can be corrected to a reasonable value. Joint analysis of current meter and CTD data allowed detection of a number of interesting processes and objects in the study area. Among them are meandering of the Subarctic Front around its branching point with formation of chains of cyclonic and anticyclonic mesoscale eddies and strong baroclinicity of velocity fields with significant difference between the thermocline and abyssal flows. Statistical characteristics of corrected "Megapolygon-87" velocities are compared with preceding measurements in the region.

1. Introduction

The importance of mesoscale processes in oceanic dynamics and their climatic applications is well recognized in recent decades. A large set of hydrophysical experiments to study mesoscale eddies and jets in energetically active regions of the world ocean have been conducted in the former Soviet Union [*Koshlyakov*, 1986]. The first well-resolved mapping of open ocean mesoscale eddies was derived from the hydrographic data of "Polygon-67" in the Arabian Sea [*Koshlyakov et al*., 1970]. "Polygon-70" [*Koshlyakov and Grachev*, 1973] in the tropical North Atlantic provided, for the first time, direct measurements of velocities in mesoscale eddy field. Data from the collaborative U.S.-USSR POLYGON Mid-ocean Dynamics Experiment (POLYMODE) in the Sargasso Sea in 1977–1978 [*Grachev et al*., 1984] allowed quantitative analysis of interactions of eddies with each other and with large-scale currents. Later, multiship expeditions "Southern Ocean-83" [*Koshlyakov et al*., 1985] conducted south of Africa, "Mesopolygon-85" [*Ivanov*, 1988] in the tropical North Atlantic, and "Alantex-90" [*Koshlyakov and Sazhina*, 1994] in the North Atlantic Current contributed to investigation of eddy dynamics and kinematics, eddy structure, etc.

Unprecedented among these projects in spatial scale and largest in utilized resources was "Megapolygon-87" (MP), conducted June–October 1987 in the northwestern Pacific (NWP) by 11 research vessels of six institutions under coordination by the P. P. Shirshov Institute of Oceanology, Moscow. Preceding direct velocity measurements by Japanese and U.S. oceanographers provided a general background for understanding horizontal and vertical velocity structure and its temporal evolution along and across the Kuroshio Extension. Results of the analysis of long-term velocity series were described by *Schmitz et al*. [1982], *Schmitz* [1987] (1980–1982 measurements at 10 moorings deployed at 27°–41°N, 152°E, 1983–1984 measurements at 6 moorings deployed at 30°–40°N, 165°E, and 2 moorings deployed at 35°N, 175°E), *Taft et al*. [1973], *Taft* [1978] (west of the South Honshu Ridge), *Taira and Teramoto* [1981] (on the ridge), *Imawaki and Takano* [1982], and *Imawaki et al*. [1984] (near 30°N, 146°E). In all these projects, sparse horizontal resolution did not allow a reliable insight into the spatial structure of the mesoscale eddy field.

The goals of MP were to study the dynamics of the Subarctic Front in the vicinity of its branching point (Figure 1), three-dimensional structure of mean currents, characteristics of mesoscale eddies of various natures, and their interaction with each other and with frontal jets, cross-frontal fluxes, and large-scale air-sea interaction processes. The two major components of MP were an array of 177 moorings and six conductivity-temperature-depth (CTD) surveys. These measurements have provided a unique data set, having resolved a number of prominent structures along with their temporal evolution. At the same time, quantitative analysis faced a problem of high errors in the velocity records, related to data contamination by wind waves. The waves acted on surface floats of the moorings, and the effect of buoys' motions spread downward along a heavily tensed wire, affecting current meters and eventually resulting in overestimation of the velocity magnitude.

In section 2 we describe the MP CTD surveys and their configuration, timetable, and data and demonstrate general features observed. Section 3 is devoted to the MP mooring array, its deployment scheme, data availability, a review of general characteristics of observed currents, the surface wave

[1]International Pacific Research Center, University of Hawaii at Manoa, Honolulu, Hawaii.
[2]P. P. Shirshov Institute of Oceanology, Russian Academy of Sciences, Moscow, Russia.
[3]Department of Physics and Physical Oceanography, Memorial University of Newfoundland, St. John's, Newfoundland, Canada.

Paper number 2000JC000436.
0148-0227/01/2000JC000436$09.00

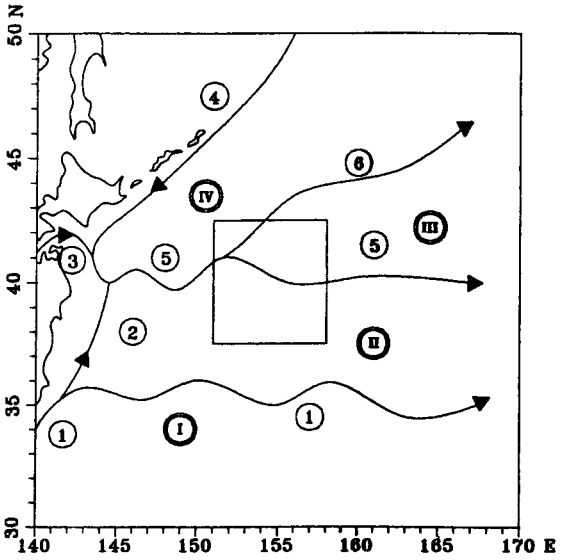

Figure 1. A circulation scheme in the frontal zone of the Kuroshio and Oyashio Currents. The MP area is framed by the square. Currents are marked as follows: 1, Kuroshio and its extension; 2, northern branch of the Kuroshio; 3, Tsugaru; 4, Oyashio (Kuril); 5, Subarctic (SC); and 6, northern branch of SC. Zones are as follows: I, subtropical; II, interfrontal; III, southern Subarctic; and IV, northern Subarctic.

effect on velocity records, and the procedure used for the velocity data correction. It also contains maps of computed mesoscale currents and results of the comparison of MP data with the velocity statistics reported in larger area by previous researchers. Results of the combined analysis of CTD and current meter data are in section 4, where we express our vision of the processes and give characteristics of the objects detected during MP in more detail. Section 5 summarizes our findings and hypotheses.

2. CTD Surveys

Figure 2 shows the scheme of all CTD stations conducted during MP. Most of the measurements were done from the sea surface through 1500 m depth. In total, 1653 profiles were collected, which can be systemized as six subsequent surveys of the study area at 20 miles (32 km) separation between stations. The first survey was conducted June 14–30, 1987, by a single ship to define the location of main fronts in the region just before the deployment of the mooring array. Others, although executed by as many as 10 research vessels, were often interrupted by storms and by the deployment, inspection, and recovering of moorings. Actually, CTD measurements were almost continuous (when it was possible), and their separation for a set of surveys is not very distinct. In this paper we take the following convention: survey 1, June 14–30; survey 2, July 20 to August 25; survey 3, September 6–17; survey 4, September 19–26; survey 5, September 27 to October 11; and survey 6, October 23 to November 1. We found that this choice gives a set of temperature maps (Figures 3 and 4) that allows us to trace major mesoscale objects and events in the MP area.

Some problems with the CTD data are caused by the variety of CTD tools used by different ships, along with poor calibration and instability of some of their sensors. The worst situation was with salinity data for deep measurements. Nevertheless, owing to large values of temperature and salinity anomalies at and around the Subarctic Front and within most mesoscale eddies of interest, we have representative temperature maps at all the depths (Figures 3 and 4) and salinity maps above 700–1000 m depth. The structure of the salinity field corresponds well with the structure of the temperature field (in the sense of positions of fronts and eddies) and, for brevity, is not shown in this paper. Figure 5 includes all MP CTD profiles and illustrates general high correlation between temperature (T) and salinity (S) at 200 m. It contains two groups of T-S points with good correlation within each of them; group A reflects continuous modification of water properties between the subtropical and subpolar water masses, and group B is discussed in section 5.

We display temperature maps at only two standard levels (125 and 1200 m), close to current meter depths of 120 and 1200 m. More maps of temperature and salinity fields are given by *Lebedev et al.* [1992]. Figures 3 and 4 illustrate the differences between frontal and eddy field structures in thermocline and in the deep layers, which were also confirmed by velocity measurements.

The large-scale structure of main fronts in the area was found to correspond qualitatively to the scheme shown in Figure 1, although the fronts expressed high variability (probably, instability) at 125 m (Figure 3) and were much broader and weaker at 1200 m (Figure 4). The Subarctic Current (SC), branching at 125 m around 41°N, 154°E, formed a quasi-meridional meander more than 200 km long and less than 100

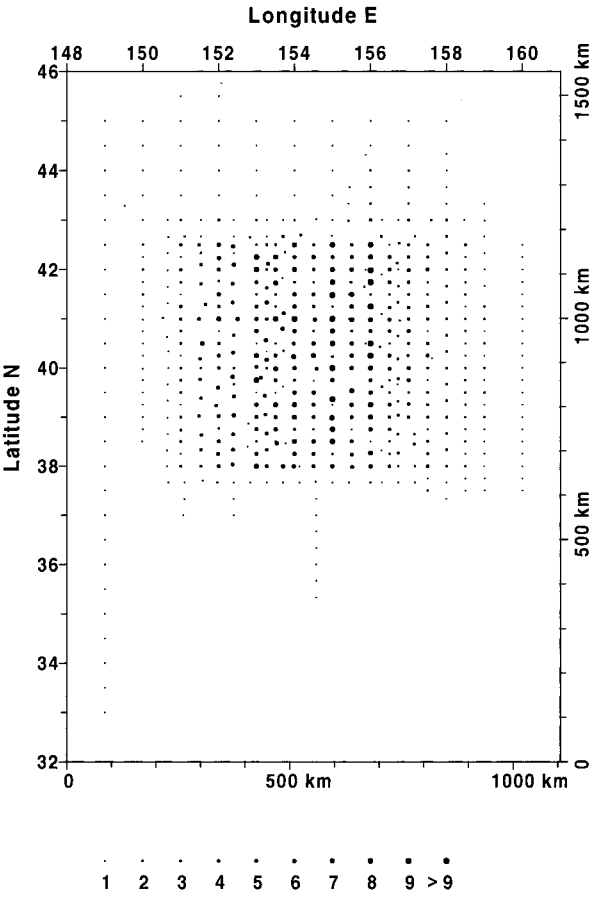

Figure 2. Location of 1653 CTD stations of MP. Symbol sizes are proportional to the number of repeat measurements.

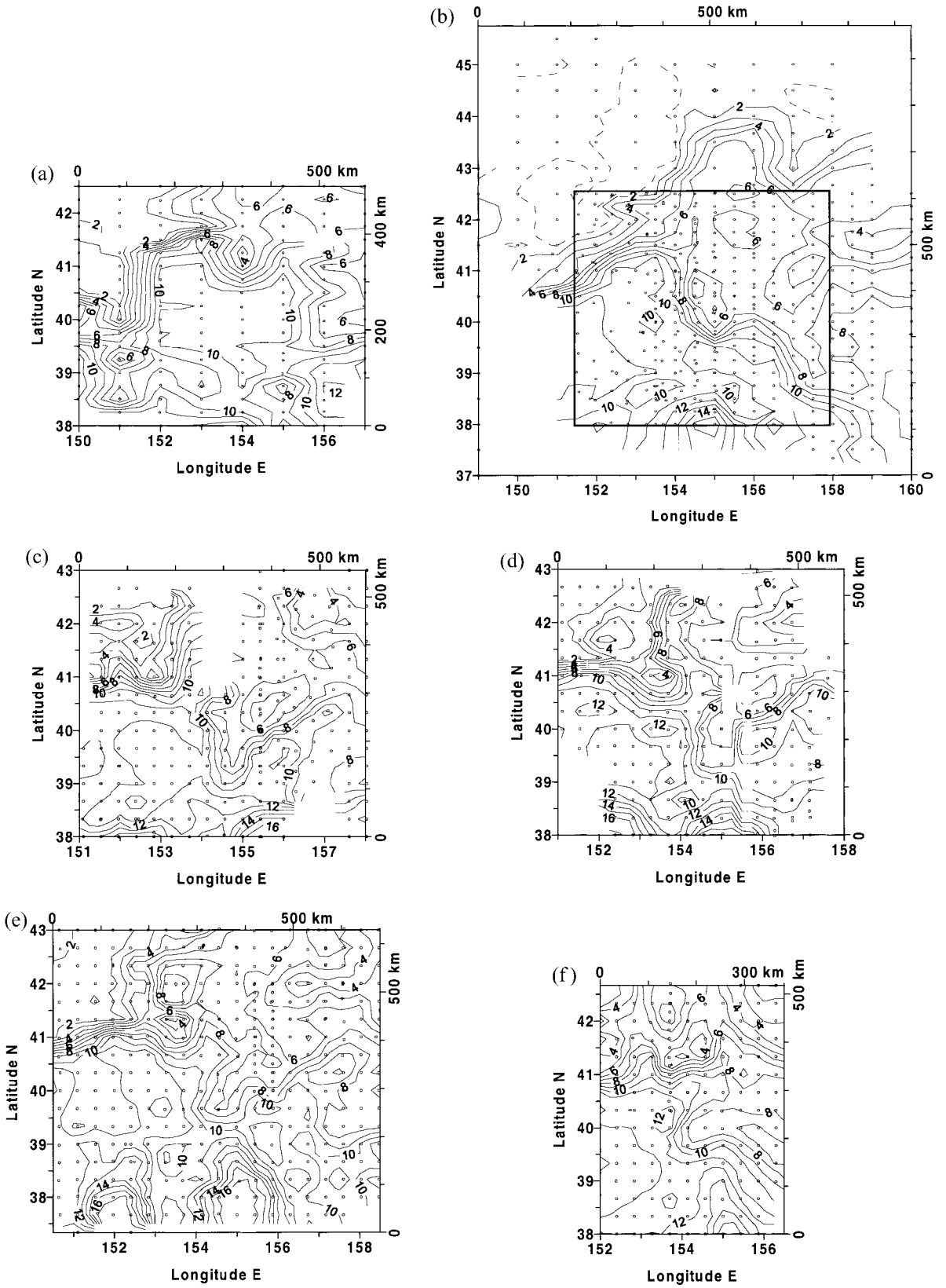

Figure 3. Temperature at 125 m for six MP CTD surveys. (a) Survey 1 (June 14–30, 1987), (b) survey 2 (July 20 to August 25), (c) survey 3 (September 6–17), (d) survey 4 (September 19–26), (e) survey 5 (September 27 to October 11), and (f) survey 6 (October 23 to November 1). Numbers are degrees Celsius. Open circles mark stations. The rectangle in Figure 3b frames the area of the MP mooring array (Figures 10–13).

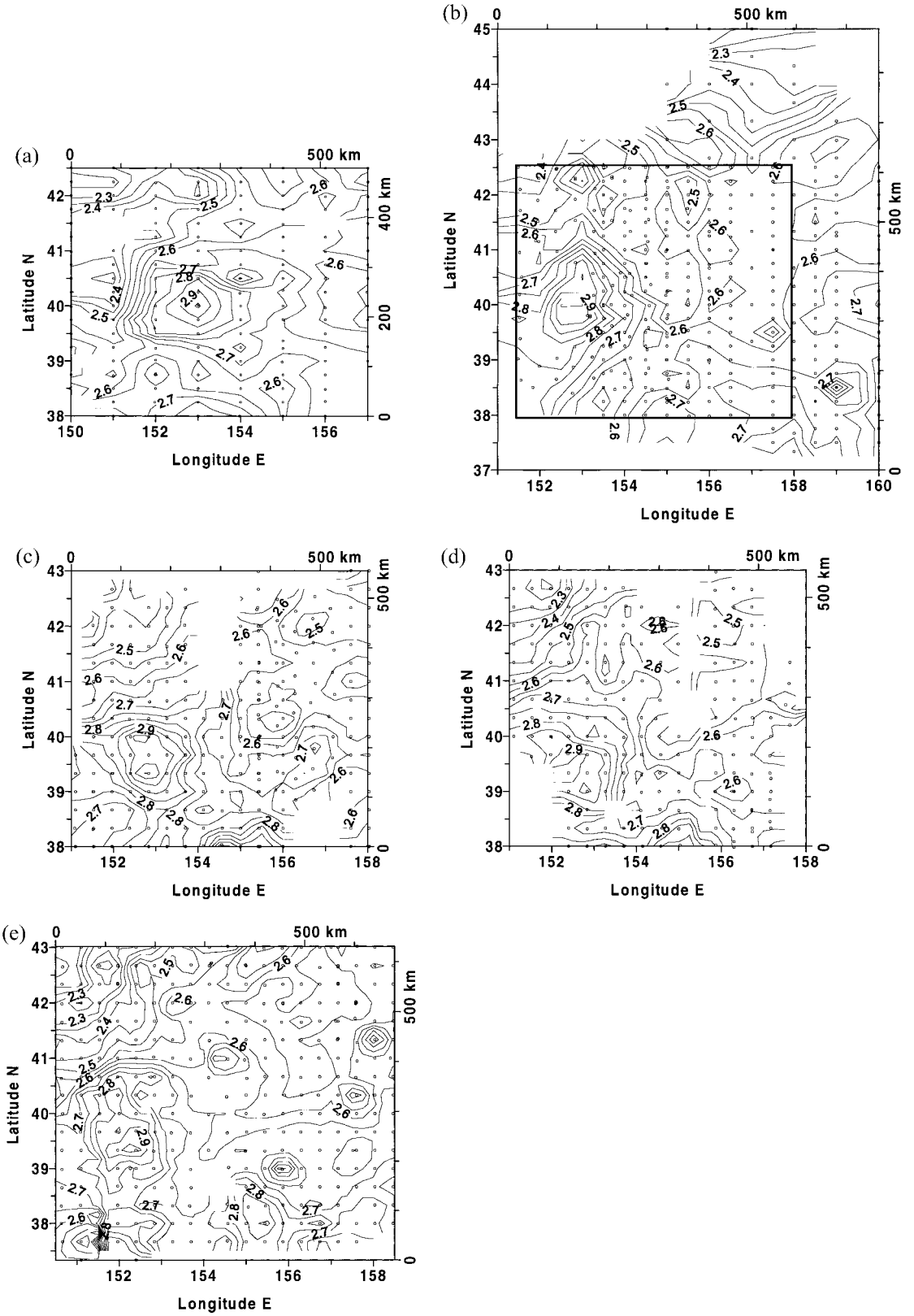

Figure 4. Same as Figure 3 but at 1200 m and for the first five CTD surveys.

km wide, which then split into a set of warm mesoscale eddies. At least three large warm eddies showed their steady signatures in the temperature field. Two of them, at the very south of MP, were the Kuroshio eddies. The third eddy, seen better in the deep layer data, had its persistent location just south of the SC splitting point (Figure 1). Characteristics of these and other objects along with their temporal evolution and physics are discussed in section 4.

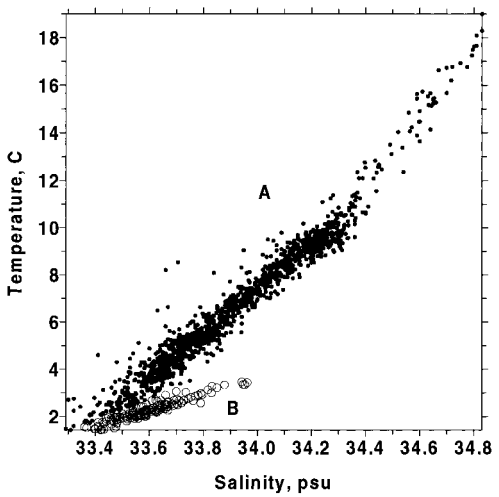

Figure 5. T-S diagram for all MP CTD measurements at 200 m.

3. "Megapolygon" Mooring Array

3.1. Array Design

Direct velocity measurements at mesoscale were done at 177 moorings deployed in an area ~500 km × 500 km centered at 40°N, 155°E. The original deployment scheme was on the triangular grid with 23 miles (40 km) spatial separation. The bottom topography (Figure 6) was rather smooth with a major depth range of 5200–5800 m, making buoy placement a relatively easy task. The array was arranged in two steps: The western subarray was deployed July 31 to August 23, 1987, and the eastern and southern buoys were added September 6–24. The array was recovered October 6–24, starting from the western side of the study area. Measurements continued for almost three months, and the maximum array configuration was maintained for 13 days (September 24 to October 6). During this time, moorings were inspected at their locations and partially recovered and/or replaced.

All the moorings were equipped with vector-averaging current meters (CM) "Potok" mounted at 120 and 1200 m levels. Buoys in two smaller clusters (Figure 7a) were also equipped with CMs at 4500 m, and in addition, buoys in the western of these two clusters carried CMs at 400 m as well. Almost all of

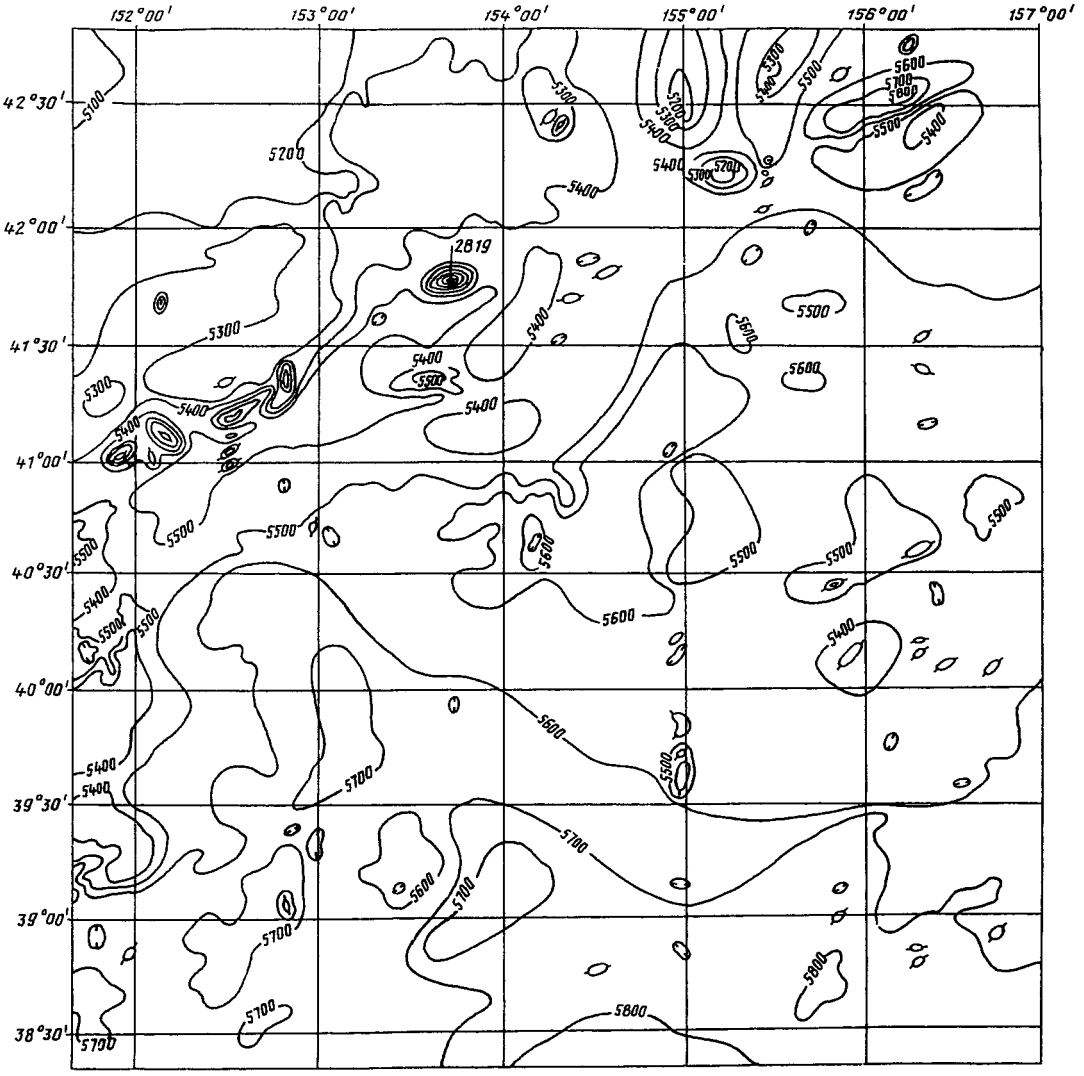

Figure 6. Bottom topography at MP area. Contour interval is 100 m.

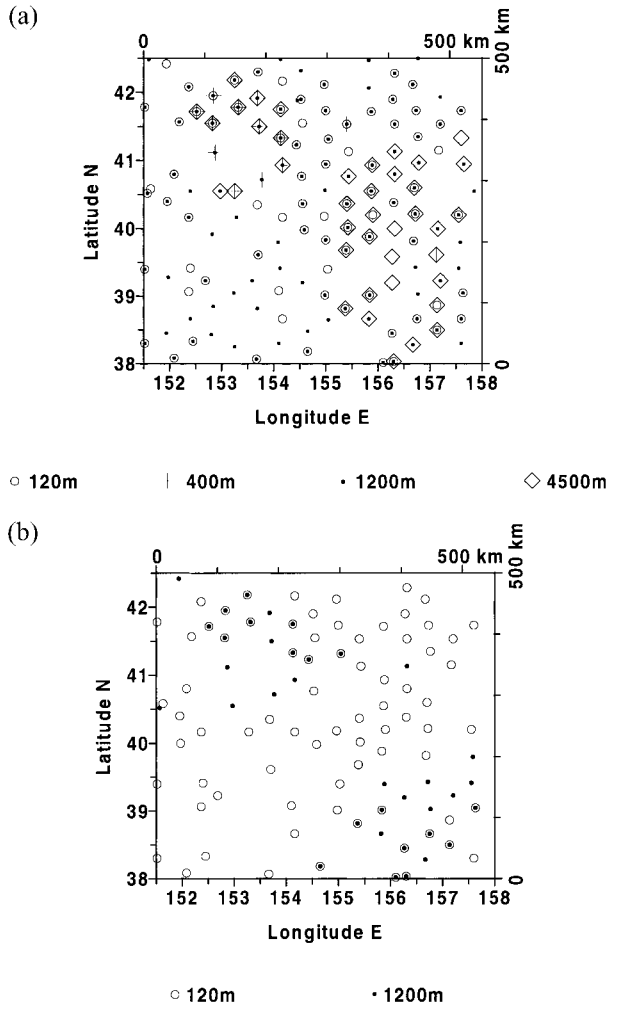

Figure 7. A scheme of location and vertical distribution of (a) velocity and (b) temperature records at the moorings.

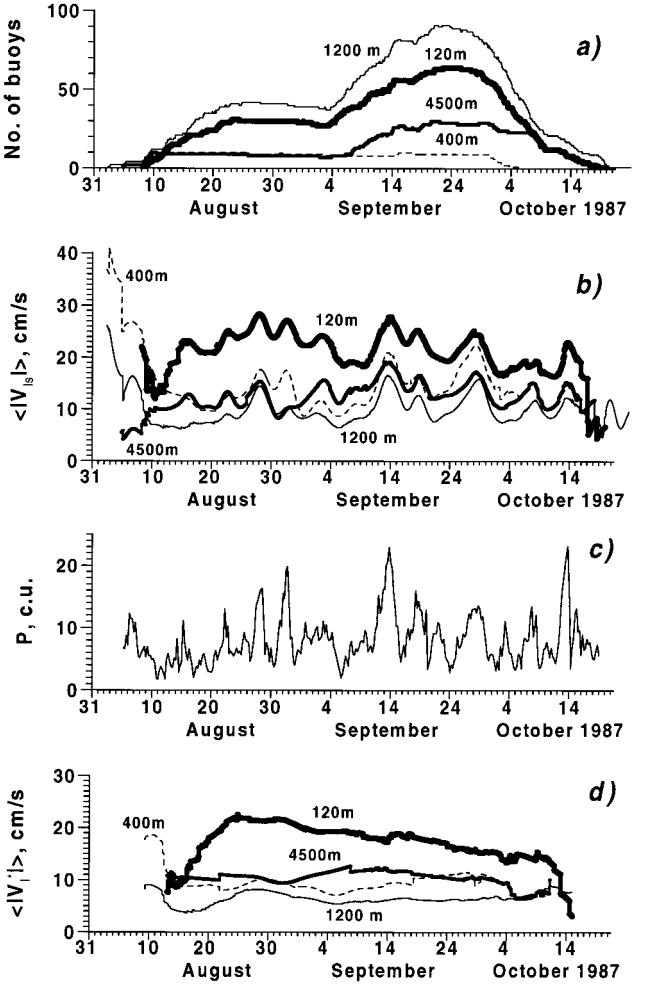

Figure 8. Number of current meters (Figure 8a), array-mean low-frequency (mesoscale) velocity magnitude as estimated from raw (Figure 8b) and corrected (Figure 8d) data at each level, and the RMS horizontal gradient of atmospheric pressure at sea level (Figure 8c). Lines in Figures 8b and 8d are discontinuous because of changes in mooring array configuration.

the 120 m CMs had temperature sensors, as did two groups of 1200 m CMs. Averaging intervals both for velocity and temperature measurement were 30 min, after which information was recorded onto magnetic tape cassettes.

Unfortunately, many moorings were lost, displaced, or found drifting because of fast currents, heavy storms, and high fisheries activity in the region. In addition, many individual CMs were lost, damaged, or malfunctioning. In total, ~51% of potential data were lost or found unusable. A location scheme of the moorings that were recovered and provided good-quality data is shown in Figure 7. The set of a quality-controlled velocity data consists of more than 400,000 records. Its complete description and illustrations are made available by *Yaremchuk et al.* [1992]. The temporal distribution of the total number of good-quality CMs at four levels is shown in Figure 8a.

3.2. Correction of Velocity Data Contaminated by Surface Wave Effect

In our study we found that velocities **V**, recorded by MP CMs, differed significantly from real velocities **V***, and this section describes our effort for their correction. For clarity of our consideration we introduce here a spectral decomposition of **V** as

$$\mathbf{V} = \mathbf{V}_{ls} + \mathbf{V}_h = \mathbf{V}_l + \mathbf{V}_s + \mathbf{V}_h, \tag{1}$$

where $\mathbf{V}_s$ is a component of **V** corresponding to temporal frequencies of the storm events over MP region and computed by 2–8 day band-pass filter; $\mathbf{V}_l$ and $\mathbf{V}_h$ are lower and higher-frequency components, respectively; and $\mathbf{V}_{ls} = \mathbf{V}_l + \mathbf{V}_s$. Analogously, we decompose real velocities **V*** and horizontal gradient P of atmospheric pressure at sea level:

$$\mathbf{V}^* = \mathbf{V}_l^* + \mathbf{V}_s^* + \mathbf{V}_h^*, \tag{2}$$

$$P = P_l + P_s + P_h. \tag{3}$$

This method is designed for evaluation of the $\mathbf{V}_l^*$ component responsible for mesoscale processes in the ocean.

Preliminary consideration of the velocity fields measured at MP revealed a strikingly high temporal variability of array-mean magnitude of low-frequency velocity $\mathbf{V}_{ls}$ (or mean speed, Figure 8b) at all four observational levels. High correlation was found between variations of $\langle|\mathbf{V}_{ls}|\rangle$ at any pair of depths and also with variations of the RMS P, calculated from digitized facsimile radiomaps, received from the Tokyo meteorological

center and averaged over the MP area (Figure 8c). Each peak in $\langle|\mathbf{V}_{ls}|\rangle$ (Figure 8b) agrees with some storm event or typhoon passage, which are clearly seen in P peaks in Figure 8c.

It has been shown by *Maximenko* [1992] that measured velocities $\mathbf{V}_{ls}$ intensified up to 150% during rough weather conditions and principal changes were in the velocity magnitude, not in its direction, which varied significantly between the observational levels because of the baroclinicity of the currents at MP. Increase and decrease of the velocity magnitude at any depth were synchronous with increase and decrease in wind speed over the MP area. It has been found that this effect is not based on realistic physics of the oceanic currents but caused by the design of the moorings and CMs. A standard MP mooring consisted of a cylindrical surface buoy, an iron wire of variable thickness with CMs mounted beside it, and heavy anchors. The length of the wire exceeded local ocean depth by 50–100 m, while the anchors had to be able to keep the mooring at the deployment point in typical hydrographic conditions. Earlier, *Gould and Sambuco* [1975] showed that surface waves can significantly force the surface buoy and its oscillatory motions can be translated downward along the tensed wire. *Panicker* [1974] found that because of turbulent friction in water, lateral displacements of the wire elements are expected to decay in the upper ocean at the scale of the vertical decay of surface waves, whereas longitudinal oscillations are able to reach the much lower CMs. In application to MP mooring design this was confirmed later by the direct measurements undertaken during "Atlantex-90" in the North Atlantic [*V'yugin et al*., 1992], which detected almost identical vertical velocities at 300 and 3000 m depths with the amplitudes corresponding to 20–30% of the estimated orbital surface wave motions. In a separate experiment with MP type of CMs it has been proved that such vertical oscillations do give rise to a significant overestimation of the measured velocity magnitude.

Efforts of MP velocity data correction (N. A. Maximenko, Technique for velocity data correction distorted by wind-wave effect, submitted to *Journal of Atmospheric and Oceanic Technology*, 2001) (hereinafter referred to as Maximenko, submitted manuscript, 2001) resulted in the method based on the following assumptions: (1) Real storm-generated motions of seawater $\mathbf{V}_s^*$ are negligible compared to recorded $\mathbf{V}_s$ values and oceanic low-frequency velocities $\mathbf{V}_l^*$. (2) Variations of the wind-wave effect are simultaneous at all moorings. (3) Wind-wave effect caused changes only in $\mathbf{V}_{ls}$ magnitude, not in its direction. (4) At storm-related timescale, wind-wave effect is proportional to P (RMS horizontal gradient of atmospheric pressure at sea level), and, hence, $\langle|\mathbf{V}_l^*|\rangle$ can be estimated as

$$\langle|\mathbf{V}_l^*|\rangle = \langle|\mathbf{V}_l| - P_1 \cdot \langle|\mathbf{V}_s|\rangle/P_s. \quad (4)$$

(5) For each time, distortion $\mathbf{V}_s$ is proportional to $\mathbf{V}_l$ that can be generalized as

$$\mathbf{V}_l^* = \mathbf{V}_l \cdot \langle|\mathbf{V}_l^*|\rangle/\langle|\mathbf{V}_l|\rangle \quad (5)$$

(where brackets denote array mean) and used for the low-frequency velocity correction.

The physical meaning of (4) is rather simple. It extrapolates measured velocities to the no-wind case $P = 0$, using $\langle|\mathbf{V}|\rangle$ to P scaling at storm-related frequencies. $\langle|\mathbf{V}_l^*|\rangle$, calculated from (4), is shown in Figure 8d. It is discontinuous because of temporal changes in the mooring array configuration.

Each assumption listed above is supported by the results of careful analysis of MP data (N. A. Maximenko, submitted manuscript, 2001). It has been shown that corrected velocities agree well with CTD data in terms of vertical shear of geostrophic velocities, horizontal advection of thermal anomalies, and overall data assimilation in the quasi-geostrophic numerical model. These studies gave 10–20% as an error estimate in $\mathbf{V}_l^*$.

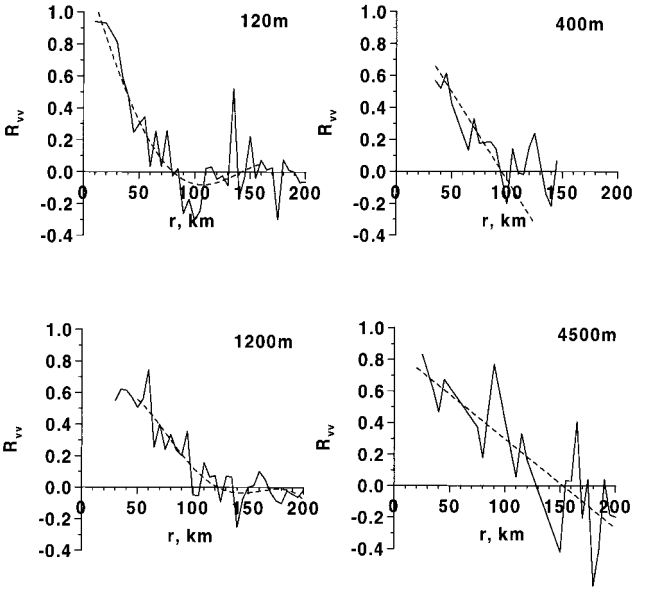

Figure 9. Spatial velocity autocorrelations at observational levels.

3.3. Characteristics of Velocity Field

Although the difference between Figures 8b and 8d is large, some statistical features derived from measured and corrected velocities appeared to be qualitatively similar. For example, the fact that surface waves contributed mainly to the magnitudes of measured velocities, not to their direction, allowed us to obtain reliable estimates of spatial and temporal scales as well as to detect the events of eddy appearance, stretching, and decay directly from the raw data. Also, the correction has not changed much the relative kinetic energy distribution between the depths.

Velocity horizontal autocorrelation functions calculated for each depth are displayed in Figure 9. It is seen that the scale of the velocity field grew gradually from 75 km at 120 m to ~150 km at 4500 m level. For the deepest, 4500 m, level this estimate is less accurate because of poor statistics in the horizontal (the mooring array resolved only one to three mesoscale velocity field features at a time).

In the vertical, the highest velocity correlation has been found between two upper (120 and 400 m) levels (90%, Table 1). The calculation was done using the corrected data from pairs of CMs, mounted at the same mooring. Although correlation between other pairs of neighboring levels was also rather high (59% for 400–1200 m and 66% for 1200–4500 m), correlation between the deepest (4500 m) and the two upper (120 and 400 m) levels was missing or even negative (−19% and −11%, correspondingly). This result is confirmed by similar calculations for 19 moorings with simultaneous velocity records available at three levels: 120, 1200, and 4500 m (Table 2). The only significant difference between Tables 1 and 2 is as much as 2 times lower correlation between velocities at 120 and those at 1200 m (27.5%). As will be seen in section 4, this

Table 1. Statistics of Corrected Velocity Calculated for Moorings With CM Data Available Simultaneously at Pairs of Levels

Level	Parameter	120 m	400 mm	1200 m	4500 m
Single-level statistics	Number of CMs	71	12	106	36
Single-level statistics	Number of records	93,292	22,071	131,324	39,951
Single-level statistics	$\langle u_{l^*} \rangle$, cm/s	2.8 ± 1.7	2.6 ± 1.6	−0.8 ± 0.5	−4.0 ± 1.7
Single-level statistics	$\langle v_l^* \rangle$, cm/s	−0.72 ± 1.7	1.9 ± 3.1	−0.6 ± 0.4	−1.5 ± 0.8
Single-level statistics	$\langle u_l^{*\prime} 2 \rangle$, cm^2/s^2	188 ± 30	32.7 ± 8.4	26.7 ± 2.7	82 ± 23
Single-level statistics	$\langle u_l^{*\prime} \cdot v_l^{*\prime} \rangle$, cm^2/s^2	5.3 ± 24	8.4 ± 10.4	1.9 ± 1.7	4.8 ± 4.5
Single-level statistics	$\langle v_l^{*\prime 2} \rangle$, cm^2/s^2	206 ± 28	69.0 ± 41	23.8 ± 2.1	23.6 ± 3.7
400 m	Number of CMs	4			
400 m	Number of records	5670			
400 m	Velocity vector correlation coefficient	0.90 ± 0.07			
1200 m	Number of CMs	61	9		
1200 m	Number of records	76,131	21,967		
1200 m	Velocity vector correlation coefficient	0.53 ± 0.07	0.59 ± 0.08		
4500 m	Number of CMs	21	9	34	
4500 m	Number of records	25,017	16,233	41,953	
4500 m	Velocity vector correlation coefficient	−0.19 ± 0.16	−0.11 ± 0.21	0.66 ± 0.07	

difference is due to the variety of observed jets and eddies with different baroclinic structure, whose location and evolution defined variations in velocity correlation in space and time.

Negative values or lack of correlation between velocities measured at 120 and 4500 m along with almost opposite directions of the mean velocity vectors at these levels point at a very different origin and nature of currents in the upper and deep ocean at MP. As is seen from Table 2, the mean velocity at 120 m was east-northeastward, whereas at 4500 m it was directed west-southwestward. This can be interpreted as a manifestation of a deep countercurrent. In addition, both mean and eddy kinetic energy (as can be seen from mean velocities and their standard deviations in Tables 1 and 2) were found to be larger at 120 and 4500 m than at intermediate, 400 and 1200 m, levels. This may indicate coexistence of two forcing mechanisms: wind-driven circulation in the upper ocean and the large-scale topography-controlled thermohaline circulation in the deep layers.

Direct comparison of MP data with the preceding measurements is difficult since only two moorings were deployed previously within the MP array area, i.e., WP1 moorings 695 (at 41°N, 152°E with CMs at 300, 600, 1200, 4000, and 5800 m) and 696 (at 39°N, 152°E with CMs at 600, 1200, and 4000 m) [*Schmitz*, 1987]. In 1980–1982 there were two year-long settings at each site, but severe data loss occurred for all CMs of the second setting of mooring 696 and for the first setting of CMs of mooring 695 at 300 and 1200 m. At first glance, there are three significant differences between the WP1 and MP parameters displayed in Tables 1 and 2; that is (1) eddy kinetic energy (EKE) at intermediate and deep levels was 1.5–3 times larger at MP, (2) at WP1, EKE decayed fast and monotonically with depth, unlike at MP, where it was minimal at intermediate 1200 m level, and (3) off-diagonal Reynolds' stresses were negative at WP1 north of KE but varied between the depths at MP.

However, we believe that these differences can be explained by insufficient statistics of both experiments combined with interannual variations in the Kuroshio Extension–Subarctic Front (KE-SF) system. *Schmitz et al*. [1982] and *Schmitz* [1987] found the highest EKE in the periods 30–150 days. MP data have a corresponding maximum in the periods 40–60 days [*Yaremchuk et al*., 1992], which are longer than the time of simultaneous work of MP CMs. At the same time, MP revealed the complexity of horizontal velocity structure unresolved by WP1 data. Only velocities at 120 and 1200 m depth are available in the western part of the MP array close to the WP1

Table 2. Statistics of Corrected Velocity Calculated for the Moorings With CM Data Available Simultaneously at 120, 1200, and 4500 m Levels

	120 m	1200 m	4500 m
Number of CMs	19	19	19
Number of records	21,021	21,021	21,021
$\langle u_l^* \rangle$, cm/s	5.5 ± 2.9	−1.5 ± 1.1	−4.2 ± 2.6
$\langle v_l^* \rangle$, cm/s	1.3 ± 3.4	−0.5 ± 1.1	−2.2 ± 1.0
$\langle u_l^{*\prime 2} \rangle$, cm^2/s^2	84 ± 19	16.8 ± 4.2	78 ± 21
$\langle u_l^{*\prime} \cdot v_l^{*\prime} \rangle$, cm^2/s^2	−5.0 ± 6.2	1.6 ± 0.6	13.5 ± 4.0
$\langle v_l^{*\prime 2} \rangle$, cm^2/s^2	209 ± 48	15.8 ± 3.1	25.0 ± 5.7
Velocity vector correlation coefficient			
1200 m	0.28 ± 0.15		
4500 m	−0.21 ± 0.17	0.59 ± 0.08	

moorings locations. Exact position and configuration of SF during WP1 are not known, while differences between two settings are remarkable. Whereas overall mean abyssal velocity averaged over moorings 695 and 696 is westward, in agreement with later observations north of KE along 165°E [*Joyce and Schmitz*, 1988], its value varies significantly between the CMs and their settings. In all the cases, dispersion of the abyssal zonal velocity component is 2–3 times larger than that of the meridional component, corresponding well with our Tables 1 and 2. Simultaneous estimates of EKE are possible at WP1 only for the first setting of mooring 696. They give ~20 and 35 cm^2/s^2 for 1200 and 4000 m [*Schmitz*, 1984] and are in good agreement with our Table 1 for 1200 and 4500 m depths. A distinctive event of "bottom intensification" of the velocity is found in the mooring 704 data obtained during WP1 at 27°N, 152°E [*Schmitz et al*., 1982], where mesoscale velocities at 5900 m were highly coherent with those at 4000 m but 30% more energetic. Similar intensification can be seen also in Figure 2 of *Imawaki et al*. [1984]. Analogously to MP levels of 120 and 400 m (Table 1), *Schmitz et al*. [1982] found a high (0.9) coherence between WP1 velocities at 250 and 500 m. At these levels, overall mean velocity tends to be directed eastward [*Schmitz et al*., 1987] with high variability between the settings and the CMs.

For further analysis we used corrected CM velocity data to calculate a horizontal stream function Ψ at all four levels. For this purpose, we employed variational technique minimizing the following cost function:

$$\mathbf{F} = k \cdot \int (\Delta\psi)^2 \, ds + \sum [\mathbf{I}([\nabla \times \psi]) - \mathbf{V}_l^*]^2, \qquad (6)$$

where $\mathbf{I}$ is a local linear operator, interpolating gridded velocity from the apexes of the grid cell onto the measurement point, $\mathbf{V}_l^*$ are the corrected velocities, ∇ is the horizontal gradient vector, Δ is the horizontal Laplacian operator, and k is the only adjustable parameter. Coefficient $k = 0.01$ has been chosen to provide the balance between smoothing at the scale of separation distance between the moorings and fitting to corrected velocities at 10% accuracy. Summation in (1) is done over all CM data available at a time, and integration is performed over the interpolation area. We calculated ψ on a regular grid with a 5 km spacing in the horizontal at 0000 and 1200 GMT each day, when the data set was sufficient. A quasi-Newtonian descent algorithm of *Gilbert and LeMarechal* [1989] was used.

Weekly maps of stream functions at all four levels, calculated this way, are plotted in Figures 10–13. The velocity field contains numerous eddies and jets with their meanders generally well resolved by the observational array and agreeing with CTD surveys. Description of the maps is addressed in section 4.

4. Structures and Processes Detected at MP

In this section we undertake a combined analysis of the CTD and mooring array data to give a comprehensive description of the spatial structure of fronts, jets, and eddies at mesoscale.

4.1. Main Fronts at "Megapolygon-87"

The structure of the main fronts around the MP area agrees well with the scheme in Figure 1. It is illustrated best by Figure 3b, which shows the largest survey, survey 2 (July 20 to August 25, 1987). The Subarctic Front (SF) is very sharp at 125 m in the east part of MP. It separates 10°C warm modified subtropical water in the south from 2°C cold subpolar water in the north and is oriented east-northeastward. At 41.5°N, 153.5°E, SF splits into two branches separated by the 6.5°C isotherm. The northern branch (NSF) proceeds northeastward, whereas the southern one (SSF) makes a turn to the southeast. Subpolar water north of SF is highly uniform, with temperature contrast less than 1°C at 125 m. On the contrary, regions between the branches and south of SSF contain multiple thermal anomalies ranging in horizontal size from 300 km to the separation distance between CTD stations. As we will illustrate later, larger anomalies correspond mainly to baroclinic mesoscale eddies of various natures, while the smaller-scale ones are produced by frontal instability, eddy interaction, stirring, and, possibly, vertical motions at the fronts, all contributing to a large-scale mixing process. Temperature at 125 m varied typically between 3° and 9°C in the Southern Subarctic Zone (zone III in Figure 1) and between 8° and 17°C in the interfrontal zone (zone II in Figure 1). The warmest anomalies in the south part of MP were associated with two large anticyclones originating, probably, from the Kuroshio Extension.

Velocity data at 120 m show the Subarctic Current (SC) as a fast (20–30 cm/s) jet well seen in the west of the mooring array with its location and orientation coinciding exactly (Figure 10) with the position of SF, described above. Although splitting of SC is less clear because of eddy activity, two jets of similar strength can always be found around SF branches. Branching of SC is clearly seen on the map of September 18, 1987 (Figure 10), with a splitting point location at 41.5°N, 153.5°E. While the northern jet was rather stable, with only its velocity direction varying from northeastward on August 14 to northward on September 11, the southern one exhibited fast meandering and strong interaction with eddies of various sizes.

The velocity pattern in NSF at 400 m (Figure 11) is qualitatively similar to that at 120 m, except for velocity magnitudes, which decreased to 10–15 cm/s, and fast variations in the direction of the velocity vector on September 4–18. The small number of CMs at this depth does not allow saying for sure if SC was missing or just displaced at that period, but high (90%) correlation between velocities measured at 120 and 400 m (Table 1) suggests that principal features in the vicinity of NSF are the same at both levels.

Thermal signature of SF and its splitting for SSF and NSF persisted through the deepest layers surveyed at MP. This can be illustrated by two meridional sections taken west and east of the SF branching point. Deep isotherms shallowing northward can be found close to the SF location at 40.3°N, 149°E (Figure 14) and near SSF and NSF at 40°N and 43.8°N, 156°E (Figure 15). At the same time, fronts in the deep layers were broader in the horizontal, and their thermal contrast was weaker relative to temperature anomalies associated with mesoscale eddies (Figure 4b).

The structure of the velocity field at 1200 m was mainly determined by a number of large eddies (Figure 12) and exhibited more temporal variability than that at 120 m. In early August and early October 1987 a northeastward current with speed of 5–10 cm/s can be found at the location of NSF. Between these dates the flow pattern changes tremendously with SC directed either southeastward (maps for August 28 to September 4 in Figure 12) or southwestward (September 18).

As we discussed in section 3.3, there was no correlation between velocities measured at 120 and 4500 m at the same locations. Figure 13 for 4500 m also supports this result. Cur-

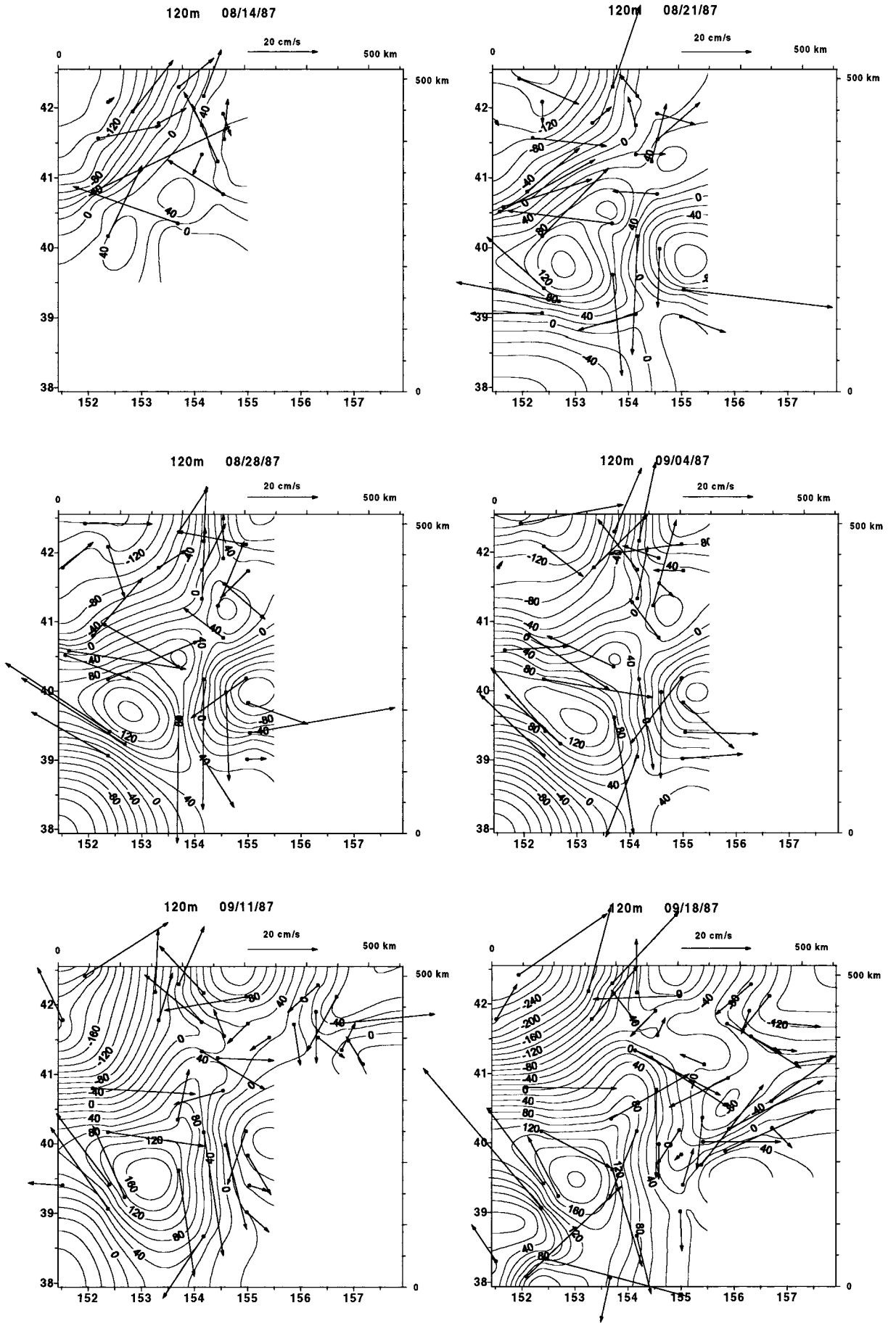

Figure 10. Weekly stream function maps at 120 m. Symbols and arrows show CM locations and corrected velocity vectors, computed as described in section 3.2. Numbers are 10^6 cm^2/s.

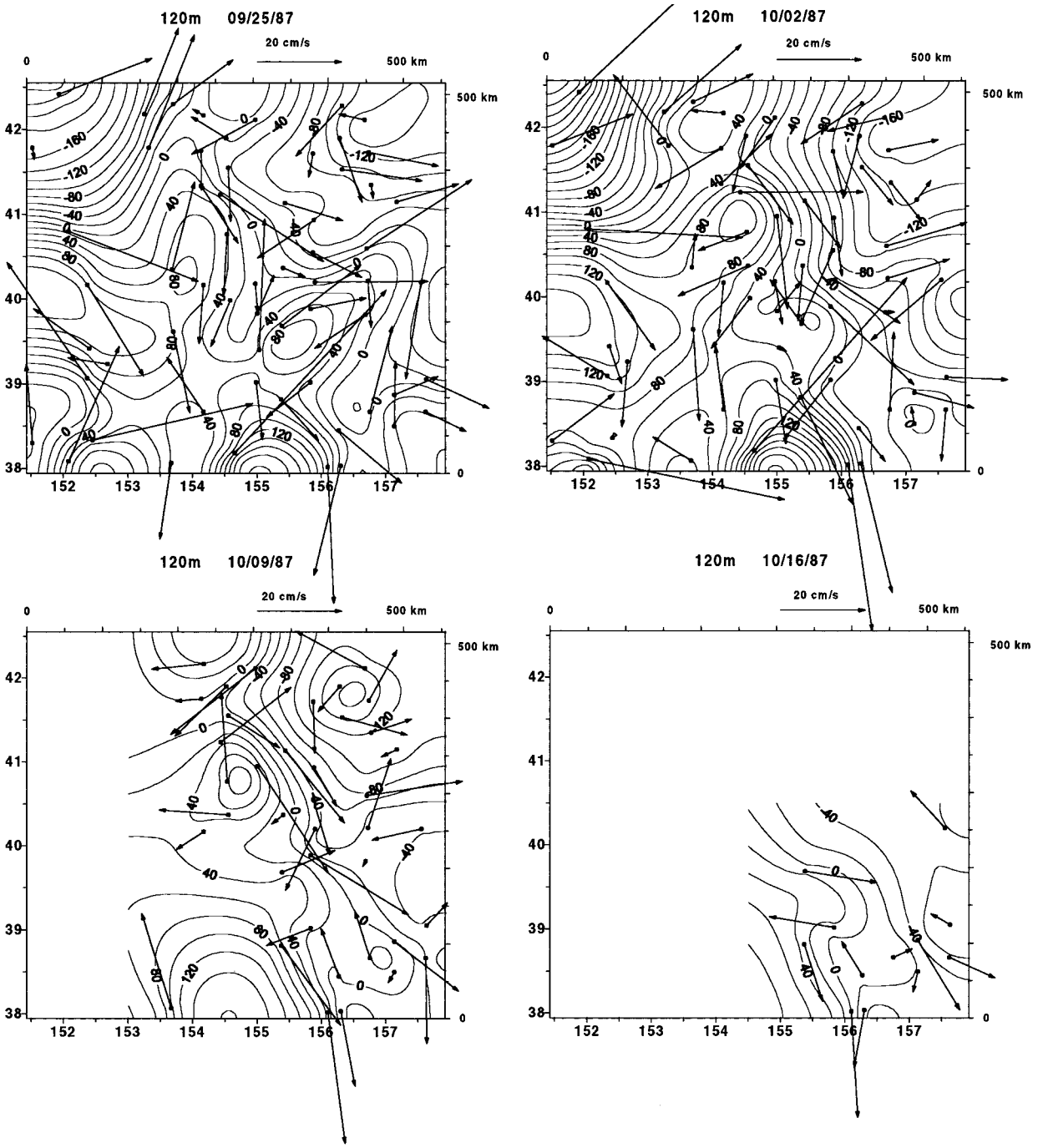

Figure 10. (continued)

rents with 20 cm/s velocities were directed either westward or southwestward in the northwestern corner of MP (NSF region) and persistently opposite to the flow at 120 m.

A frontal structure different from the one presented in Figure 1 was found in the uppermost mixed layer (not shown in the figures). The SF there was seen clearly, and at 40.5°N, 151.5°E it split or widened similarly to deeper layers. However, east of 154°E, NSF turned abruptly to the southeast, merging back with SSF around 39°N, 155.5°E. Unlike in the layers underneath, subpolar water in the mixed layer north of SF was not horizontally uniform. At 150°E the meridional temperature gradient reached 1°C per 1°N between 41° and 45°N and was probably determined by air-sea interaction. This zonality north of SF remained through 154°E, where all the isotherms turned more or less southeastward and some of them even joined SF, increasing its thermal contrast. As an illustration, the coldest isotherm in SF, outcropping at the sea surface near 149°E (Figure 14) is 16°C, whereas it is at least 1°C colder (15°C) at 156°E (Figure 15).

Another important front in the vicinity of MP is the Kuroshio Extension (KE). Although KE was beyond the MP area, its influence was very strong, mainly through warm anticyclonic eddies having detached from KE earlier. These eddies possessed large thermal anomalies and high orbital velocities.

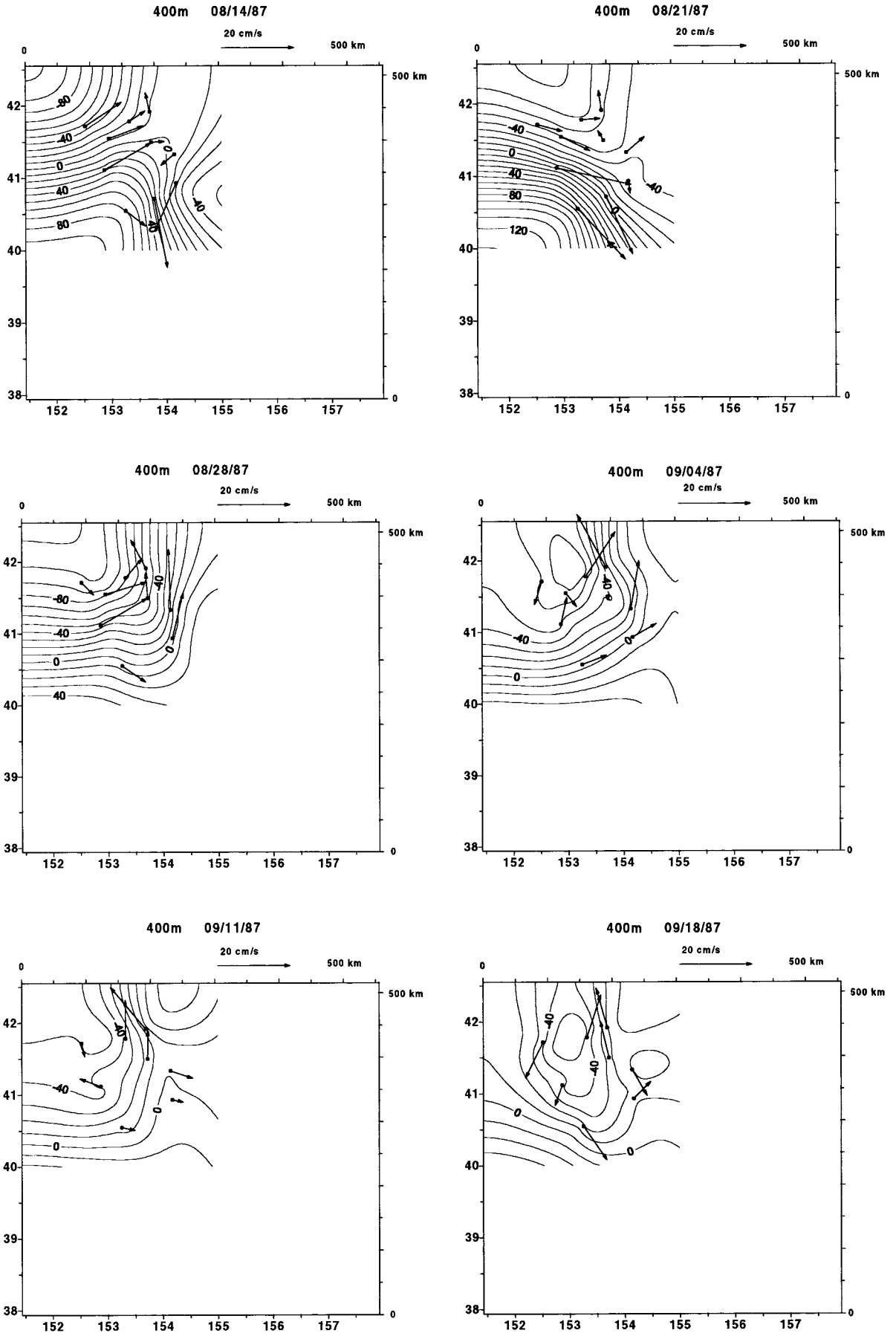

Figure 11. Same as Figure 10, but for 400 m. Numbers are 10^6 cm^2/s.

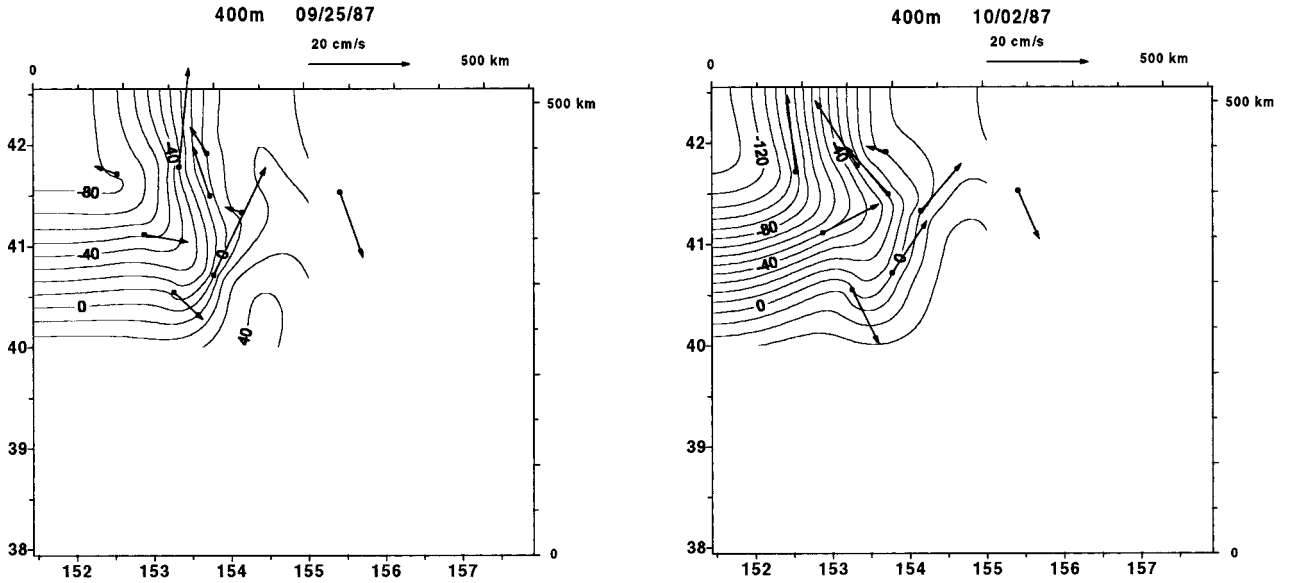

Figure 11. (continued)

They supplied the region with subtropical water from the south. Location of KE during the MP period can be estimated from two meridional sections. In August (Figure 14) the KE front was located around 35.5°N. At 149°E it was well expressed in the meridional temperature gradients in the depth range from 30 to 1000 m. The northern edge of KE at 154.5°E in late October to early November (Figure 16) was located around 35.3°N. At this section a large (250 km in size) detached eddy was detected just north of KE, with its pronounced thermal signal seen everywhere from the sea surface through 1000 m. Just to the north of that eddy there was another semi-detached warm-cored one, smaller (200 km) in size, with a weaker temperature anomaly, penetrating the MP region from the south. The latter eddy is clearly seen in Figures 3 and 4 and will be described in more detail in section 4.2.2.

The KE-SF frontal structure described in this section was not steady, but varied intensively, showing a number of interesting features. The most remarkable among them was the formation and evolution of quasi-meridional meander of SSF in late July to early October 1987. Sequential maps of its appearance at 125 m are shown in Figure 3b–3f. In August (Figure 3b) the path of SSF was rather straight with relatively weak disturbances, which can be characterized by a 250 km along-front wavelength and approximately 50 km cross-frontal displacement. However, in the first half of September (Figure 3c) the meander of SSF started to develop northward at 153.8°E, just east of the SF branching point. Two to three weeks later (Figure 3d), it was already seen as a narrow (less than 100 km wide and more than 250 km long) filament having penetrated the Southern Subarctic Zone (zone III in Figure 1) through 42.7°N. As a result of stretching, the meander became unstable and split into a set of warm anomalies of various scales. The largest of them is still seen on the October temperature maps (Figures 3e and 3f).

This meander also manifested itself in the velocity field at 120 m (Figure 10), although its signature there is less clear because of the nonuniform spatial distribution of CM data. Disagreement between smooth streamlines and individual velocity vectors indicates the presence of numerous smaller-scale eddies, not resolved by observational grid. However, one can recognize the chain of anticyclonic eddies located between 40°N, 153°E and 42.5°N, 155°E on maps of August 21 through September 11, 1987. The 20–40 cm/s fast jets at the western and eastern edges of the eddy chain outline the meander whose northern crest is beyond the array area. It is difficult to decide only from the velocity data if the meander was formed by the eddy chain or if the eddies emerged as a result of the meander instability. If the later scenario is correct, then this is a large lateral velocity shear that might cause the instability of the meander.

The strongest eddy in the chain occurred at the tail of the meander. It is seen on 120 m maps (Figure 10) from August 28 through October 9 as an anticyclone propagating westward from 155° to 154°E along the northern boundary of the array region with orbital velocities exceeding 20 cm/s. Positive thermal anomalies in that eddy at 125 m can be seen in Figures 3d–3f. Although the meander is missing in velocities at 1200 m (Figure 12) as a whole, a strong anticyclone was detected at the same time just beneath the above-mentioned eddy. Its maximum orbital velocities were ~10 cm/s and did not vary much as it drifted westward and evolved. Hence the eddy had well-developed barotropic and baroclinic components.

Ivanov et al. [1992] computed the geostrophic stream function at 120 m depth relative to a 1050 m reference level using historical data for the season of August through October. They found SC splitting and looping in the MP area in a way similar to that described above, and they hypothesized seasonal existence of the meander. At least two alternative scenarios of the meander appearance can be suggested on the basis of MP data, which are not related to the seasonality.

The first one is the meander formation by a strong interaction between two anticyclonic eddies, residing in late August—early October 1987 (Figure 10) around 39.5°N, 153°E and 42.5°N, 154°–155°E, respectively. A saddle point separating these two anticyclones appears in the stream function field, and SSF loops northward around the northern eddy. Then anomalous warm water being advected northward by the current at the western edge of these eddies could form the meander.

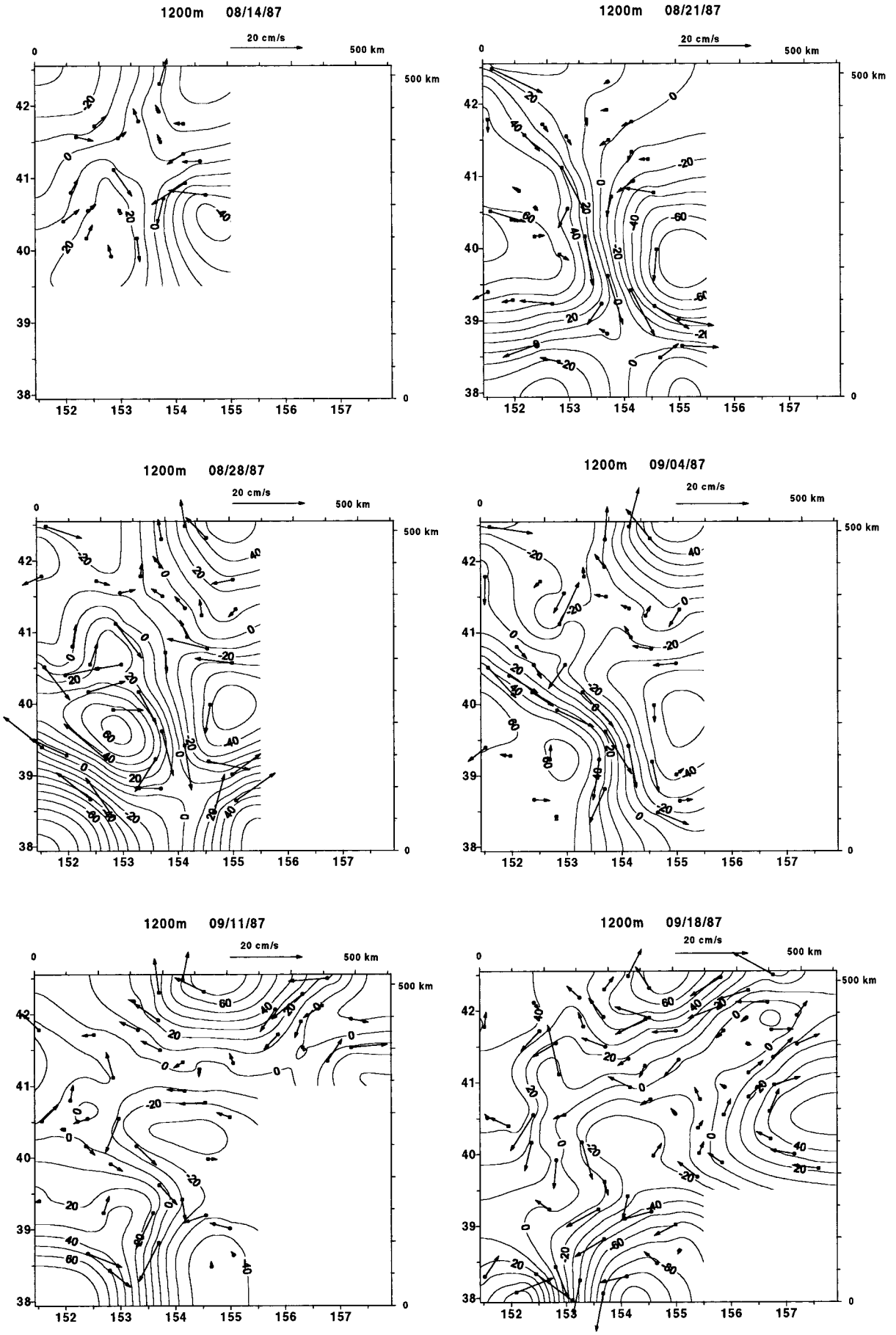

Figure 12. Same as Figure 10, but for 1200 m. Numbers are 10^6 cm^2/s.

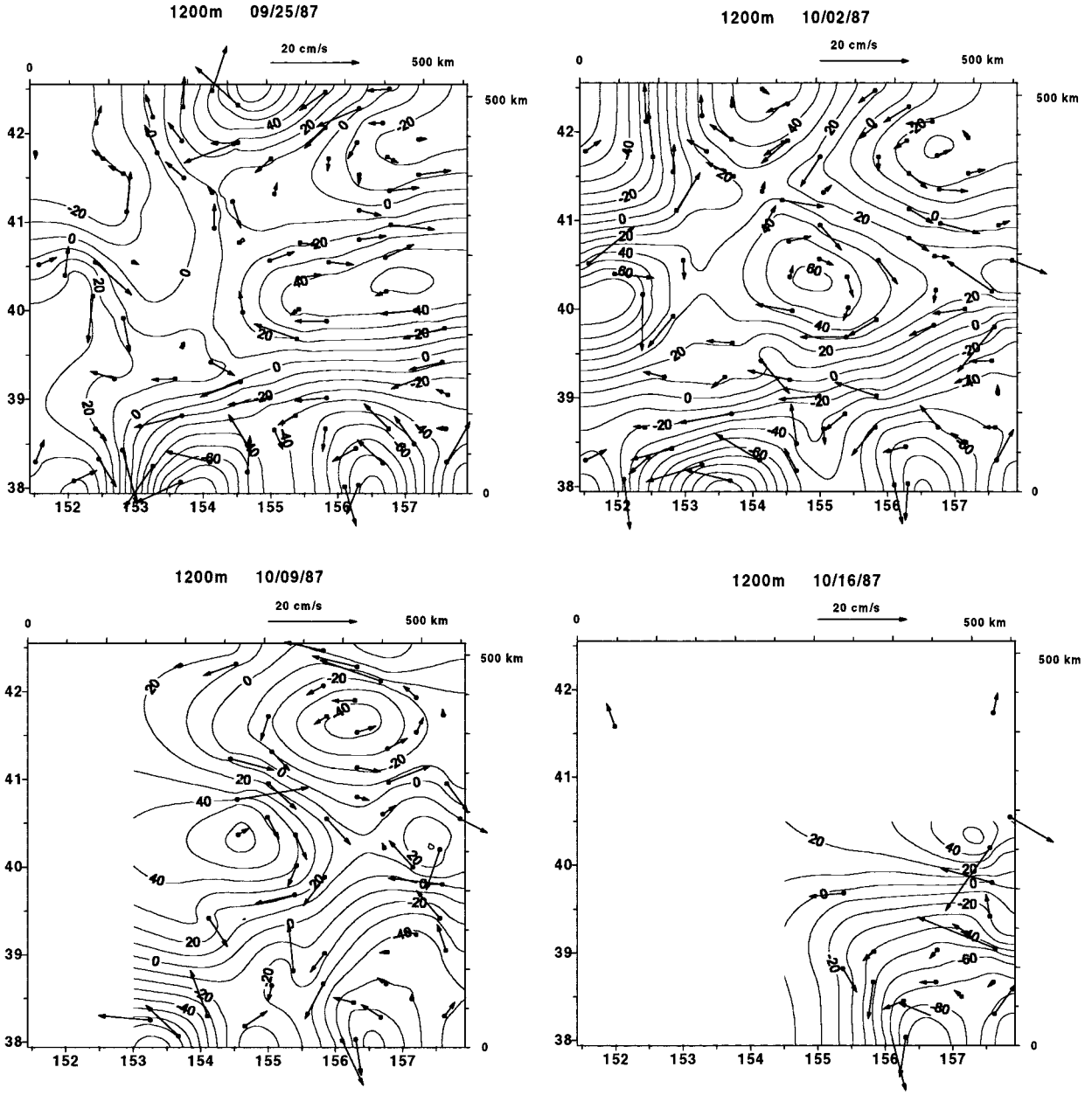

Figure 12. (continued)

The second scenario relates the meander to a larger-scale instability process in the MP interfrontal zone. One can find in Figures 3b–3e another warm SSF meander developing northward around 40°N, 156°E and two meander troughs (or cold meanders) carrying water southward around 39.7°N, 155°E (Figure 3b) and 38.5°N, 157°E, correspondingly. Similarly to the meander described above in this section, they spread ~200 km northward or southward, carried comparable temperature anomalies, exhibited strong instability, and eventually disintegrated into smaller-scale features. It is interesting that location and northward propagation of the two southern warm anomalies of subtropical water (around 38°N, 152° and 155°E, Figures 3b–3f), associated with KE eddies, agree well with location and development of the SSF meanders. If it is not a simple coincidence, then we might have detected not a meandering of a single SSF, but a complex instability of the KE-SF frontal system as a whole. *Koshlyakov et al*. [1992a] found a similar structure, analyzing CM data, and they managed to classify all the variety of mesoscale eddies observed during MP into three quasi-meridional chains of cyclones and anticyclones with their locations qualitatively corresponding to the meanders' crests and troughs described here.

4.2. Mesoscale Eddies at "Megapolygon-87"

In section 4.1 we revealed an important role mesoscale eddies play in the dynamics of the KE-SF frontal zone. In sections 4.2.1–4.2.4 we review the properties of a variety of eddies observed at MP. Their general parameters are assembled in Table 3.

4.2.1. Main anticyclone. The central part of the MP area was occupied by a strong warm-core anticyclonic eddy (WAE), clearly seen on temperature maps of all six CTD surveys at

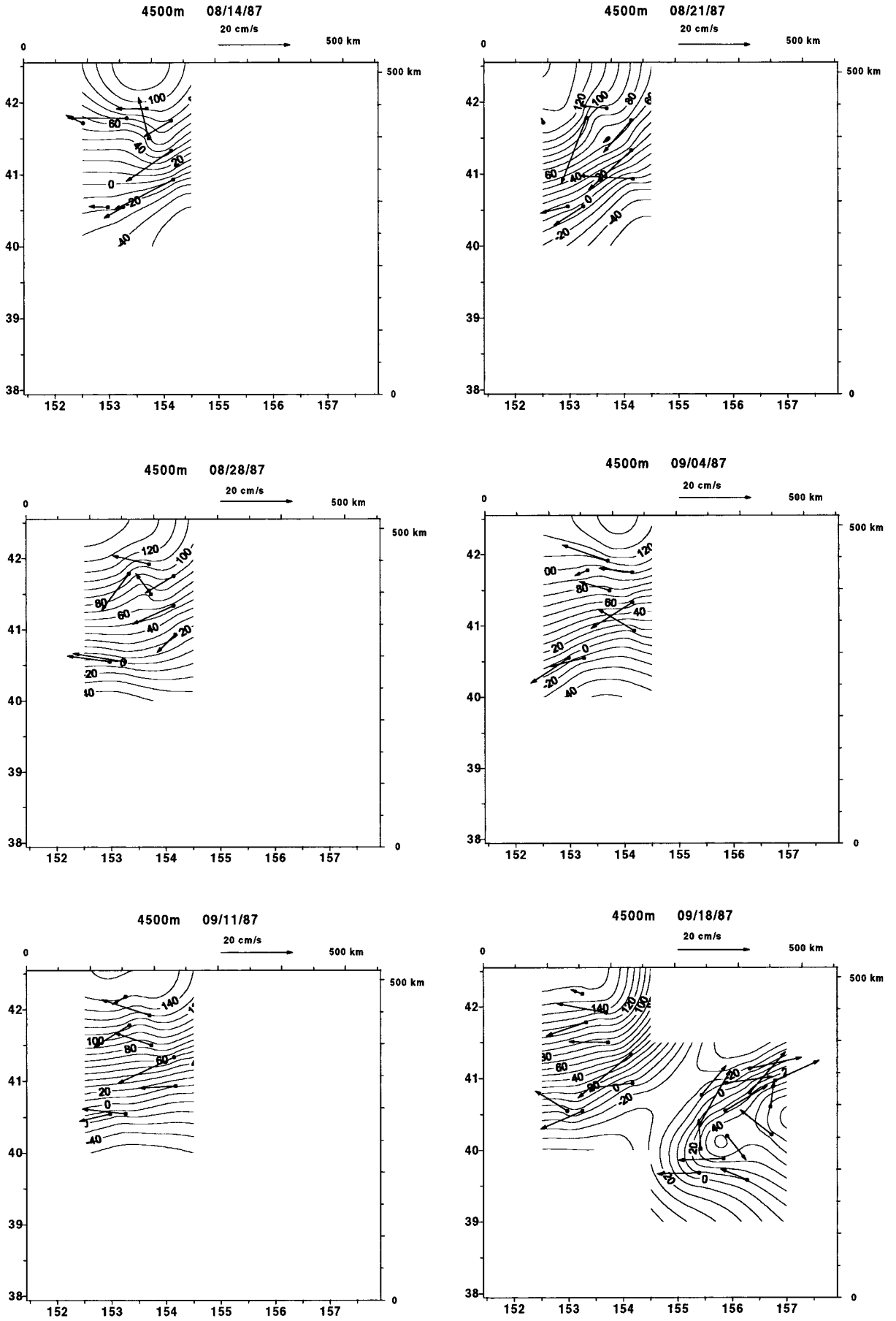

Figure 13. Same as Figure 10, but for 4500 m. Numbers are 10^6 cm^2/s.

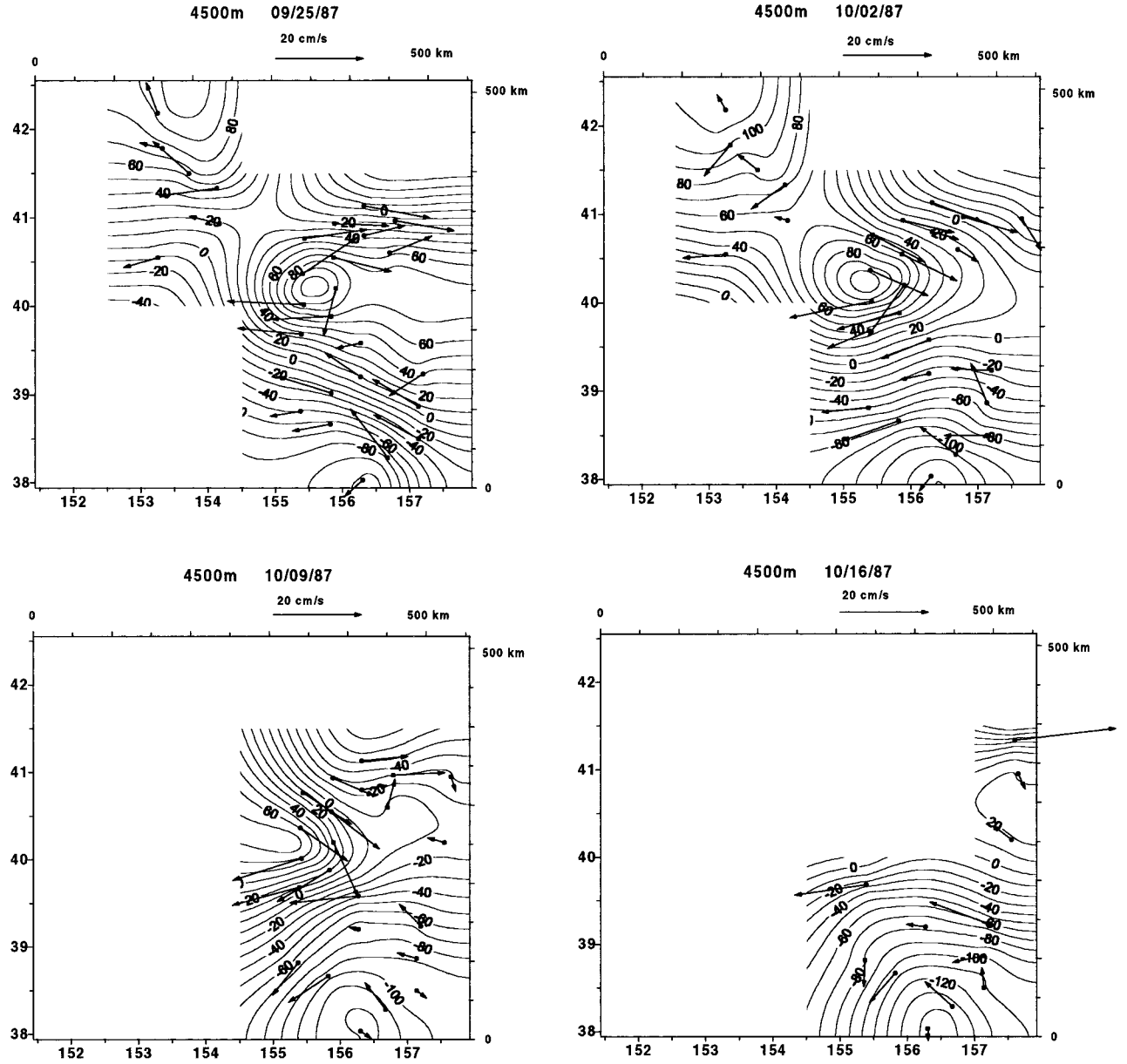

Figure 13. (continued)

1200 m (Figure 4), with its center located around 40°N, 153°E in June–August and around 39.3°N, 152.5°E in October 1987. Temperature in its core reached almost 3°C at maximum that was 0.2°–0.3°C warmer than that in the surrounding waters. The characteristic horizontal size of the anomaly was ~200 km, and its shape varied significantly during observations. The meridional CTD section along 153°E, collected June 19–23 (38°–42.5°N) and August 13–14 (42°–45°N) (Figure 17), revealed that the WAE anomaly had a complex structure above 100 m, whereas below this depth, isotherms were depressed at the eddy center all the way down to 1600 m. At 125 m its signal was still not very clear. Although survey 1 (Figure 3a) found a large 2°C warm anomaly at a nearby location in June, subsequent surveys did not reveal it, and the presence of WAE can be supposed only from development of a warm streamer that penetrated the eddy periphery from the west along 40.3°N (Figure 3c) in early September and then spiraled clockwise through October (Figures 3d and 3e). The streamer could be a manifestation of the processes responsible for modification of the cores of frontal eddies.

On the velocity maps, WAE is seen continuously from August 18 to September 23 at 120 m (Figure 10) and from August 22 to September 1 at 1200 m (Figure 12) with maximum orbital velocities of 30–40 cm/s at 120 m and 10–15 cm/s at 1200 m. As seen on the stream function map at 120 m (Figure 10) on September 4, WAE stretched in the westward direction along 40°N. The same stretching can be found in Figures 4c and 4d for temperature at 1200 m in September, when the eddy is already absent from the velocity pattern at 1200 m. Either its size decreased, it disappeared, or the vertical structure of its velocity significantly changed. Changes in the velocity field at 1200 m started on September 4, when currents southwest of WAE weakened to 5 cm/s, so that its northeastern side became a part of the jet flowing southeastward at 15 cm/s. The jet decayed by September 11, and eventually, on September 18 it formed a much broader 10 cm/s fast southward flow oriented

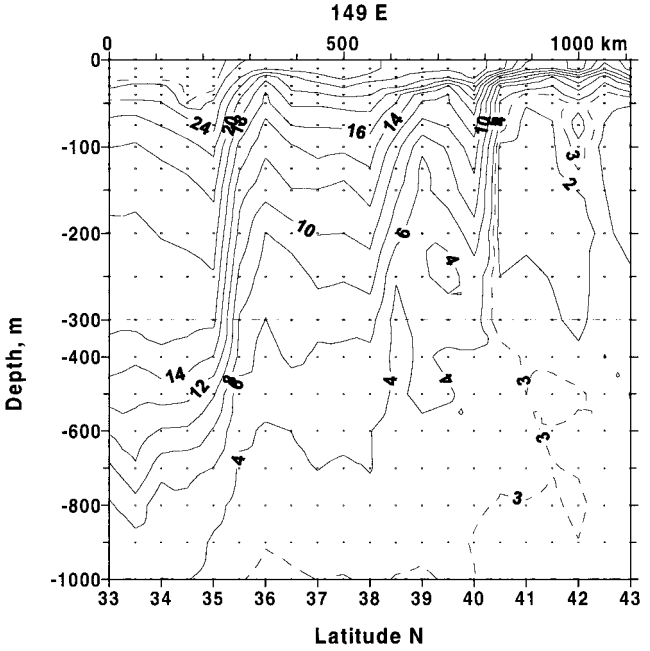

Figure 14. Temperature at meridional CTD section along 149°E, collected August 20–23, 1987, by R/V *Novoulyanovsk*. Symbols show sampling points. Numbers are in degrees Celsius.

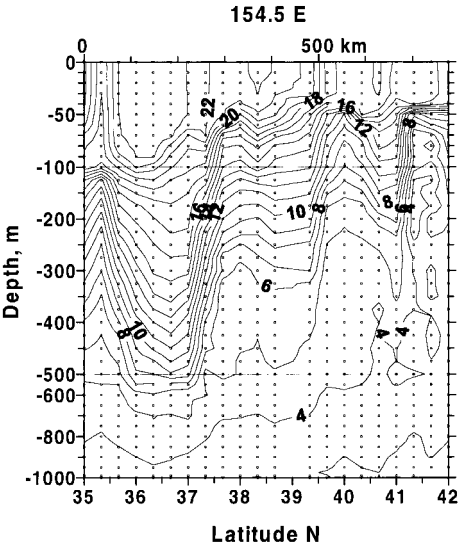

Figure 16. Temperature at meridional CTD section along 154.5°E, collected October 27 to November 3, 1987, by R/V *Dmitry Mendeleev*. Symbols show data location at standard levels. Numbers are in degrees Celsius.

just across the area of the WAE thermal anomaly. This process took place simultaneously with the SSF meander formation described in section 4.1 and also with the appearance from the east of another strong anticyclonic eddy to be discussed in section 4.2.3. Velocities, measured at 120 m, also reflect a dramatic change in WAE shape and location about September 25. Starting from that date, the eddy center can be traced farther west at 40°N, 152°E, where the anticyclone reemerged at 1200 m as well. During all that time the WAE core thermal anomaly at 1200 m survived without remarkable changes, with its center having only shifted 100 km southwestward in three months. Whereas the absence of WAE on some stream function maps can be attributed to sparse velocity data, disagreement between the eddy centers as defined from velocity and temperature data is rather clear for early October. At that time the thermal core was at the southeastern periphery of the eddy, being advected southwestward by its swirling velocities.

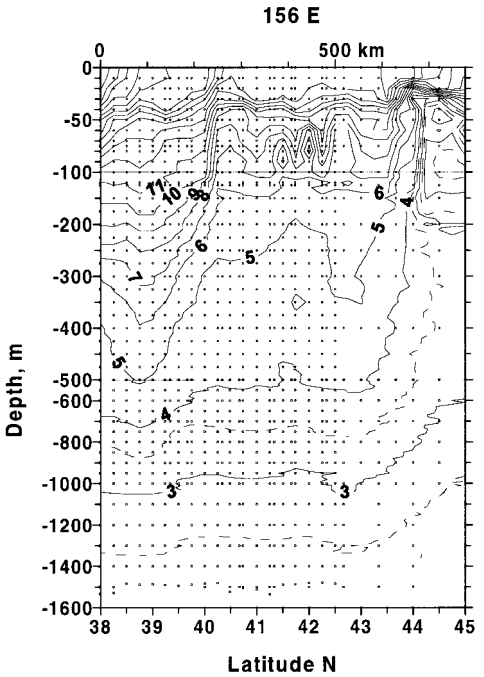

Figure 15. Temperature at meridional CTD section along 156°E, computed from stations sampled August 5–9, 1987, by R/Vs *Novoulyanovsk* and *Akademik Alexandr Nesmeyanov*. Symbols show data location at standard levels. Numbers are in degrees Celsius. Dashed lines denote 2.5° and 3.5°C isotherms.

It seems possible that WAE played an important role in the evolution of the frontal structures at MP by causing branching of SF and SC. The deep thermal structure of WAE allows us to assume that it was a ring detached much earlier from KE. High variability of velocities in the eddy in September 1987 reflects its strong nonlinear interaction with the surroundings. Survival of its thermal anomaly as well as restoration of its anticyclonic rotation must be due to its high available potential energy. An important question of persistence of WAE at this location or its periodic replacement with a newer ring needs further investigation. At the same time, it seems probable that it was the WAE interaction with another anticyclone, located at 42.5°N, 154°–155°E (section 4.1), that initiated the warm meander crest formation of SSF.

4.2.2. Kuroshio Extension eddies. Beginning in August–September 1987, two warm temperature anomalies were seen at 125 and 1200 m (Figures 3 and 4) in the south of the MP at 152° and 155°E. As they spread north to 38°N by the end of September their maximum temperatures reached 17°C at 125 m and 2.7°C at 1200 m, corresponding to 6° and 0.2°C warm anomalies. Sections along 153°E (Figure 17) and 154.5°E (Figure 16) revealed deflection of isopycnals in the vicinity of these anomalies within all the depth range of CTD measurements. The structure of these anomalies, although not measured extensively, indicates that they were of KE origin with subtropical water inside. Velocity observations at the southern periphery of the MP array detected strong currents reaching 50

Table 3. Main Mesoscale Eddies Observed at "Megapolygon-87"[a]

Dates and Locations (Year 1987)	Sign	Thermal Anomaly, °C (at depth, m)	Size, km (at depth, m)	Maximum Orbital Velocity, cm/s (at depth, m)	Propagation	Probable Origin
June 40°N, 153°E; Oct. 1, 39.3°N, 152.3°E	A	2. (125), 0.3 (1200)	300	40 (120), 15 (1200)	unsteady SW at 1 cm/s on average	old KE eddy
June–Aug., 45.5°N, 155°E; Oct. 9, 42.5°N, 154°E	A	3. (125, at the eastern edge of the eddy), unclear (1200)	200	25 (120), 10 (1200)	unsteady W at 1 cm/s on average	unclear
July–Oct., 38°N, 155°E	A	6.0 (125), 0.2 (1200)	150	50 (120), 15 (1200, see section 4.2.2)	almost steady (weak N)	KE eddy
Sept.–Oct., 38°N, 152°–153°E	A	6.0 (125), 0.2 (1200)	150	40 (120) 15 (1200, see section 4.2.2)	unclear (weak N and W)	KE eddy
Sept. 17, 40.5°N, 157.5°E, Oct. 13, 40.5°N, 154.8°E	A	missing	300 (1200), 200 (4500)	10 (1200), 20 (4500)	W at 8.5 cm/s	barotropization, instability of deep flow, flow interaction with bottom topography
Aug. 20 to Sept. 19, 40°N, 155°E	C	−2.0 (125), −0.15 (1200)	300 (120), 200 (1200)	30 (120), 15 (1200)	unclear	unclear
Sept. 17, 42°N, 157°E; Oct. 11, 41.8°N, 155°E	C	unclear	150–200	20 (120), 10 (1200)	W at 3 cm/s	meandering local jet

[a]Notations are as follows: A, anticyclone; C, cyclone; SW, westward; N, northward; W, westward.

cm/s at 120 m and 10–15 cm/s at 1200 m at the edges of the anomalies, with meridional components being in good agreement with the anomalies' locations. The best illustration of this can be obtained by comparing the 120 m stream function map for October 2 (Figure 10) with the temperature field at 125 m (Figure 3e), where the features do look like warm-core anticyclonic eddies. On other days, correspondence is less clear both because of insufficient data and because of presence of smaller-scale disturbances.

A striking contrast to the flow pattern at 120 m is that at 1200 m (Figure 12). Instead of anticyclones, described for the upper level, there are two distinct cyclonic eddies with centers displaced zonally half a wavelength with respect to the thermal anomalies, so that the warm anomaly at 155°E just separates the cyclones. Kinematically, this difference can be explained by the existence of a fast westward jet at 1200 m near 39°N, just north of the eddies. Indeed, if the eddy velocity field can be schematically approximated by a zonal chain of eddies composed of a periodic sequence of steady vortices of both signs and equal strength, then adding a mean westward flow will intensify cyclones and weaken anticyclones in the north part of the chain. On the contrary, mean eastward flow at 120 m would amplify anticyclonic eddies there. This idea is supported by the October 9 map (Figure 12), showing that after the decay of the jet at 1200 m an anticyclonic structure emerged at 38°N, 155°E.

At the same time, it is also possible that deep cyclones are induced by anticyclonic thermocline eddies as the latter develop northward [*Koshlyakov et al*., 1992b]. However, the question raised earlier in section 4.2.1, as to how distinct thermal anomalies were able to survive being in disagreement with the local horizontal velocity field, is still open.

4.2.3. Deep anticyclone. One of the largest eddies detected at MP was an anticyclone, seen on September 18 to October 9, 1987, stream function maps at 1200 m (Figure 12). Zonally, it extended by 300 km with meridional size of 200 km. The eddy was formed at the edge of the MP or entered the MP region from the east on September 16 and propagated westward along 40.4°N at phase speed 8–9 cm/s. Characteristic orbital velocities were 10 cm/s. Just beneath this eddy a strong anticyclone of similar shape was observed in currents at 4500 m (Figure 13), that anticyclone was smaller in size and bounded by two jets, 15–20 cm/s fast and 150 km broad. The eddy had no clear signature in the temperature field at any depth. Its intensification with depth indicates formation in the deep layers, possibly by meandering jets or by flow interaction with bottom topography.

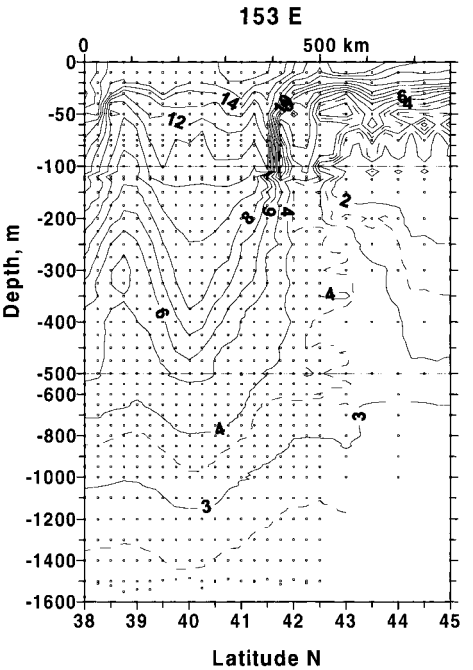

Figure 17. Temperature at meridional CTD section along 153°E, computed from stations sampled June 19–23, 1987, by R/V *Akademik Alexandr Nesmeyanov* (38°–42.5°N), on July 30, 1987, by R/V *Akademik Kurchatov* (41°N), and on August 13–14, 1987, by R/V *Novoulyanovsk* (42°–45°N). Symbols show data location at standard levels. Numbers are in degrees Celsius. Dashed lines denote 2.5° and 3.5°C isotherms.

Koshlyakov et al. [1992b] pointed out that deep eddies at MP could be a product of the barotropization process. Both the large size of the eddy and prevailing zonal velocities match the theory [*Rhines*, 1977]. *Koshlyakov et al*. [1992b] estimated that the rate of westward drift of the eddy agreed well with a phase speed of linear barotropic Rossby waves. Actually, maps in Figure 12 for the intermediate (1200 m) depth give a unique illustration of complex interaction between baroclinic eddies of different vertical structure.

4.2.4. Cyclonic eddies at "Megapolygon-87." Although anticyclones were more distinct and stable at MP and their role in the dynamics of frontal zone looks dominant, a comparable number of various size cyclonic eddies were observed there as well. Their description and classification are complicated by their typically smaller size and faster evolution and decay and also by a weak or missing thermal signal in their cores that made it difficult to detect cyclones by hydrographic observations. That is why we focus here on only two cyclones.

One of them was observed from the very beginning of velocity measurements in early August through the middle of September 1987. With its center at 40°N, 155°E both at 120 and 1200 m (Figures 10 and 12) the cyclone had maximum orbital velocities of 20–30 cm/s at 120 m and 10–15 cm/s at 1200 m, and an original size of 300 km at 120 m and 200 km at 1200 m depth. Located between strong jets and anticyclones, it stretched and quickly disappeared. The eddy's core at 125 m was composed of 5°C water, ~2°C colder than its surroundings, and was distinct in August (Figure 3b). In September the eddy stretched and became a part of the SSF meander trough (Figures 3c and 3d). By October it disappeared as a local temperature minimum (Figure 3e). In temperature the same process can be traced at 1200 m with some time lag. At this depth the anomaly was the most clear in the beginning of September (Figure 4c) with the lowest temperature below 2.5°C. After that it stretched and decayed within a month (Figures 4d and 4e). Subpolar water found in the eddy's core might be an indication of its recent formation by meandering of NSF.

Another cyclone was induced by meandering jet in the northeastern corner of MP at the end of September 1987 (Figures 10 and 12). It emerged simultaneously with the deep anticyclone described in section 4.2.3. The cyclone is seen on October 9 maps as a large eddy at 41.7°–41.9°N, 156.2°–156.4°E, bounded by the jets reaching 20 and 10 cm/s at 120 and 1200 m, respectively. Orbital velocities grew continuously with radius and reached their maxima within the jets. Only a weak temperature anomaly can be found at a near location (Figures 3e and 4e).

5. Summary and Discussion

The analysis of "Megapolygon-87" data, based upon comprehensive observations of mesoscale processes in the Subarctic Front–Kuroshio Extension frontal zone, revealed complex structure and dynamics of fronts, jets, and eddies interacting strongly with each other and evolving at timescales from one week to several months. The MP provided dense coverage with moorings and CTD observations over an unprecedentedly large region. It has been found that features cascaded almost continuously in spatial scale from the separation distance between stations (typically, 32 km) to the length of the study area (more than 1000 km). On the one hand, that did not allow detailed description of numerous submesoscale lenses and vortices detected in the region (e.g., *Maximenko and Yamagata* [1995] and *Maximenko and Shcherbina* [1996]; see also Figure 4e) that seem to be formed by instability of fronts as well as by stretching and decaying mesoscale eddies. On the other hand, it made difficult the investigation of large-scale flow and corresponding meridional eddy heat and momentum fluxes. *Koshlyakov et al*. [1992c] have shown that estimates of the northward eddy heat flux are highly sensitive to the definition of mean flow. Its value at 120 m ranged between 0.6 and 13.0 J/(cm^2 s) depending on the mean flow model with formal confidence limits of 5–6 J/(cm^2 s).

When working with MP data, we faced an additional problem related to velocity overestimation by the current meters. The analysis, based on the careful study of the behavior of measured velocities during storm events, gave rise to a method for data decontamination (see section 3.2) at low frequencies.

The general pattern of the main fronts at MP agreed well in the 100–1200 m layer with the scheme in Figure 1, showing a SF branching point around 41.5°N, 153.5°E. This branching could be either governed by processes of scale larger than the size of the MP area or induced by local internal dynamics of SF, i.e., by SF interaction with an old KE eddy (section 4.2.1). Another feature found close to the splitting point of SF is a seamount at 41.8°N, 153.7°E (Figure 6). Being 2600 m in height with its top only 2819 m below the sea surface, it definitely disturbed deep currents. Its effect is seen on the 4500 m stream function maps in Figure 13 as fast-varying and relatively small scale disturbances of the velocity vectors, measured by neighboring CMs. Nevertheless, the small horizontal scale of the mountain and the lack of coherent velocity disturbances at upper levels make the effect of bottom topography on the SF structure questionable.

It is also not clear if the northward meander of SSF, whose formation, evolution, and decay were observed during MP and described in section 4.1, is a persistent or regularly appearing feature. Among possible mechanisms of its generation there can be the effect of another anticyclonic eddy detected at 45.5°N, 155°E in June–August 1987. Its interaction with the main MP anticyclone could force SSF to shift its path northward with subsequent northward advection of warm waters. At the same time, simultaneous existence and development of two quasi-meridional SSF meanders (with two of their crests and two of their troughs within the MP area) along with good correspondence of their locations to positions of two warm KE eddies give an idea of larger-scale instability processes of the SF-KE system as a whole. In addition, penetration of cyclonic eddies with cold subpolar water to the very south of the MP region indicates a possibility of NSF meandering, so that the observed development of SSF meanders can be just a phase of more complex SSF-NSF system dynamics.

The intensive nonlinear interaction between the jets and eddies that densely populate the MP area made the temperature and velocity fields very dynamic with a wide spectrum of spatiotemporal scales. That did not allow us to separate their evolution into a clear set of independent events or processes. In a number of situations during an interaction event the velocity field in an eddy's core was strongly disturbed and lost geostrophic coherence with temperature anomalies for several days. In most of these cases the eddy's thermal core survived almost unchanged and eventually restored the geostrophic velocity structure, probably by spending a part of its available potential energy. Similarly, velocities at 1200 m (Figure 12) were not coherent with temperature anomalies (Figure 4) in the vicinity of two southern KE warm eddies (section 4.2.2).

This can also be a result of too sparse a mooring array and a simple interpolation scheme.

Group B of points in Figure 5 can be a signature of vertical motions. Most of them differ in properties from subpolar water and are found on the cold side of NSF and WAE, indicating a secondary circulation in their vicinity. That means that the wave-like structure of the eddy field seen in Figures 14–17 and known to be common for the SF-KE region [*Vasilev and Makashin*, 1993] may exist not only because of the isotherms depression in the cores of anticyclonic eddies but also because of upwelling at their periphery, often observed by marine biologists.

Three-dimensional circulation in the region is even more complex. MP data confidently revealed differences in velocity structure at the upper 120 m and the lower 4500 m levels. The deep circulation pattern increases in strength with depth and tends to compensate thermocline circulation. A wide variety of baroclinic eddies observed at MP, with their cores in shallow and deep layers and differing in their size, origin, and, probably, dynamics, along with their strong and extremely complicated interaction at intermediate depths, outlines a prospect of long and difficult study needed for adequate description and understanding of the physics of frontal zones.

Acknowledgments. This research was partly funded by Frontier Research System for Global Change. This is SOEST contribution 5409 and IPRC contribution 84. We appreciate the two anonymous reviewers for their very helpful comments and Diane Henderson for editing the manuscript.

References

Gilbert, J. C., and C. LeMarechal, Some numerical experiments with variable storage quasi-Newton algorithms, *Math. Program.*, *45*, 407–455, 1989.

Gould, W. D., and E. Sambuco, The effect of mooring type on measured values of ocean currents, *Deep Sea Res. Oceanogr. Abstr.*, *22*(1), 55–61, 1975.

Grachev, Y. M., M. N. Koshlyakov, D. A. Nechaev, T. G. Sazhina, and M. I. Yaremchuk, Dynamics of open-ocean synoptic eddies in the POLYMODE region, *Oceanology*, *24*(4), 417–423, 1984.

Imawaki, S., and K. Takano, Low-frequency eddy kinetic energy spectrum in the deep western North Pacific, *Science*, *216*, 1407–1408, 1982.

Imawaki, S., K. Taira, and T. Teramoto, Mesoscale current fluctuations observed in the deep western North Pacific, *J. Oceanogr. Soc. Jpn.*, *40*, 39–45, 1984.

Ivanov, Y. A. (Ed.), *Hydrophysical Study During "Mesopolygon" Program* (in Russian), 258 pp., Nauka, Moscow, 1988.

Ivanov, Y. A., M. N. Koshlyakov, V. A. Melnikov, G. G. Panteleev, S. M. Shapovalov, and M. I. Yaremchuk, On the structure of the Subarctic Front in the Northwestern Pacific, in *Coherent Structures and Self-Organization of Oceanic Motions* (in Russian), edited by G. I. Barenblatt, D. G. Seidov, and G. G. Sutyrin, pp. 127–135, Nauka, Moscow, 1992.

Joyce, T. M., and W. J. Schmitz, Zonal velocity structure and transport in the Kuroshio Extension, *J. Phys. Oceanogr.*, *18*, 1484–1494, 1988.

Koshlyakov, M. N., Eddies in the open ocean, in *Synoptic Eddies in the Ocean*, edited by V. M. Karemkovich, M. N. Koshlyakov, and A. S. Monin, pp. 265–378, D. Reidel, Norwell, Mass., 1986.

Koshlyakov, M. N., and Y. M. Grachev, Meso-scale currents at a hydrophysical polygon in the tropical Atlantic, *Deep Sea Res. Oceanogr. Abstr.*, *20*(6), 507–526, 1973.

Koshlyakov, M. N., and T. G. Sazhina, Water circulation and a cyclonic ring in the Gulf Stream splitting region in May–June 1990, *J. Geophys. Res.*, *99*, 14,091–14,100, 1994.

Koshlyakov, M. N., L. I. Galerkin, and C. D. Hie'n, On the mesostructure of geostrophic currents in mid-ocean, *Oceanology*, *10*(5), 637–646, 1970.

Koshlyakov, M. N., Y. M. Grachev, T. G. Sazhina, and M. I. Yaremchuk, A cyclonic eddy in the Antarctic Circumpolar Current and heat transport across the Antarctic Front, *Oceanology*, *25*(6), 685–692, 1985.

Koshlyakov, M. N., G. G. Panteleev, T. G. Sazhina, and M. I. Yaremchuk, Structure and variability of the velocity field in the thermocline at "Megapolygon-87" mooring array, in *Experiment Megapolygon*" (in Russian), edited by Yu. A. Ivanov, pp. 242–250, Nauka, Moscow, 1992a.

Koshlyakov, M. N., N. A. Maximenko, G. G. Panteleev, T. G. Sazhina, and M. I. Yaremchuk, Structure and variability of the velocity field in the deep ocean from direct velocity measurements at "Megapolygon-87," in "*Experiment Megapolygon*" (in Russian), edited by Y. A. Ivanov, pp. 251–259, Nauka, Moscow, 1992b.

Koshlyakov, M. N., T. G. Sazhina, and M. I. Yaremchuk, Energy exchange between large-scale currents and mesoscale eddies at the Subarctic Front in the north western Pacific, in "*Experiment Megapolygon*" (in Russian), edited by Y. A. Ivanov, pp. 290–304, Nauka, Moscow, 1992c.

Lebedev, K. V., V. A. Melnikov, and A. I. Kharlamov, Hydrology, in *Atlas of Experiment "Megapolygon"* (in Russian), vol. 1, edited by Y. A. Ivanov and M. N. Koshlyakov, pp. 17–170, P. Shirshov Inst. of Oceanol., Moscow, 1992.

Maximenko, N. A., Influence of surface waves on the velocity measurements carried out using "Potok" current meter, in "*Experiment Megapolygon*" (in Russian), edited by Y. A. Ivanov, pp. 304–319, Nauka, Moscow, 1992.

Maximenko, N. A., and A. Y. Shcherbina, Fine structure of the intermediate waters in the north western Pacific, *Meteorol. Hydrol.*, *7*, 71–77, 1996.

Maximenko, N., and T. Yamagata, Submesoscale anomalies in the North Pacific Subarctic Front, *J. Geophys. Res.*, *100*, 18,459–18,469, 1995.

Panicker, N. N., Effect of cable material on surface mooring dynamics, *MODE Hot Line News*, *62*, 3, 1974.

Rhines, P. B., The dynamics of unsteady currents, in *The Sea*, vol. 6, pp. 189–318, John Wiley, New York, 1977.

Schmitz, W. J., Jr., Abyssal eddy kinetic energy levels in the western North Pacific, *J. Phys. Oceanogr.*, *14*, 198–201, 1984.

Schmitz, W. J., Jr., Exploration of the eddy field in the midlatitude North Pacific, *J. Phys. Oceanogr.*, *18*, 459–468, 1987.

Schmitz, W. J., Jr., P. P. Niiler, and C. J. Koblinsky, Two-year moored instrument results along 152°E, *J. Geophys. Res.*, *92*, 10,826–10,834, 1987.

Schmitz, W. J., Jr., P. P. Niiler, R. L. Bernstein, and W. R. Holland, Recent long-term moored instrument observations in the western North Pacific, *J. Geophys. Res.*, *87*, 9425–9440, 1982.

Taft, B. A., Structure of the Kuroshio south of Japan, *J. Mar. Res.*, *36*, 77–117, 1978.

Taft, B. A., A. R. Robinson, and W. J. Schmitz Jr., Current path and bottom velocity of the Kuroshio, *J. Phys. Oceanogr.*, *3*, 347–350, 1973.

Taira, K., and T. Teramoto, Velocity fluctuations of the Kuroshio near the Izu Ridge and their relationship to current path, *Deep Sea Res., Part A*, *28*, 1187–1197, 1981.

Vasilev, A. S., and V. P. Makashin, Mesoscale dynamics of Subarctic Frontal zone in the Pacific, *Meteorol. Hydrol.*, *4*, 60–68, 1993.

V'yugin, A. N., N. A. Maximenko, M. V. Petrov, S. G. Savin, and A. I. Kharlamov, Experimental investigation of the effect of surface waves on flow-speed measurements by automatic buoy stations, *Oceanology*, *32*(1), 124–128, 1992.

Yaremchuk, M. I., N. A. Maximenko, and G. G. Panteleev, Currents in the Subarctic Frontal zone of the north western Pacific, in *Atlas of Experiment "Megapolygon"* (in Russian), vol. 2, edited by Y. A. Ivanov and M. N. Koshlyakov, 132 pp., P. Shirshov Inst. of Oceanol., Moscow, 1992.

Y. A. Ivanov and M. N. Koshlyakov, P. P. Shirshov Institute of Oceanology, Russian Academy of Sciences, 36 Nahimovskii Prospect, Moscow 117851, Russia.

N. A. Maximenko and M. I. Yaremchuk, International Pacific Research Center, University of Hawaii at Manoa, 2525 Correa Road, Honolulu, HI 96822. (nikolai@soest.hawaii.edu; maxy@soest.hawaii.edu)

G. G. Panteleev, Department of Physics and Physical Oceanography, Memorial University of Newfoundland, St. John's, Newfoundland, Canada A1B 3X7.

(Received May 16, 2000; revised October 17, 2000;
accepted December 12, 2000.)